

Combustion Chemistry

Collection of reports for methane air combustion

Herman Andersson

23rd of July 2025

This collection of reports presents the collective work and exercises presented in Combustion Chemistry course held during the summer semester 2025. The reports cover theory and practical work regarding methane air combustion using tools such as Cantera, RMG and pyMars to simulate and model different combustion conditions and concepts taught during lectures.

Report Contents

1. **Exercise 1:** [Fundamental Thermodynamics and Stoichiometry]
2. **Exercise 2:** [Thermochemistry]
3. **Exercise 3:** [Reaction rates]
4. **Exercise 4:** [Adiabatic Flame Temperature for Methane]
5. **Exercise 5:** [Prediction of NO concentration at varying equivalence ratio]
6. **Exercise 6:** [Determination of ignition delay time of methane-air mixture using Cantera]
7. **Exercise 7:** [Determination of laminar flame speed of premixed methane-air mixture]
8. **Exercise 8:** [Sensitivity and path flux analysis for methane-air combustion in Cantera]
9. **Exercise 9:** [Development of a mechanism for a methane-air mixture using Reaction Mechanism Generator (RMG)]
10. **Exercise 10:** Reduction of a kinetic mechanism using pyMARS

Task 1: For a given change in enthalpy (ΔH) and change in entropy (ΔS), determine if the reaction is going to be spontaneous or non-spontaneous and qualitatively show it on the plot area provided below. If the reaction changes from spontaneous to non-spontaneous (or vice versa) at some temperature (T), calculate the temperature value and mark it on the plot.

- (a) $\Delta H = +85 \text{ kJ/mol}$ and $\Delta S = +300 \text{ J/mol K}$
- (b) $\Delta H = -150 \text{ kJ/mol}$, $\Delta S = +200 \text{ J/mol K}$ and $T = 298 \text{ K}$, calculate ΔG
- (c) $\Delta H = +75 \text{ kJ/mol}$ and $\Delta S = -100 \text{ J/mol K}$ and $T = 298 \text{ K}$, calculate ΔG
- (d) $\Delta H = -100 \text{ kJ/mol}$ and $\Delta S = -250 \text{ J/mol K}$

Answer: By calculating the Gibbs energy $\Delta G = \Delta H - \Delta TS$ and seeing if the values reach zero for any temperature will show if the reaction at any point goes from spontaneous to non-spontaneous. If $\Delta G > 0$, the reaction will be non-spontaneous. If $\Delta G < 0$, the reaction will be spontaneous. For our four cases, the calculations and figures are presented below.

(a) $\Delta H > 0$ and $\Delta T > 0$ will result in a shift for ΔG , will go from non-spontaneous to spontaneous at higher temperatures

$$\Delta G = \Delta H - \Delta ST \rightarrow 0 = 85 * 10^3 - 300 * T \rightarrow T = 283.33K \approx 283K$$

(b) $\Delta H < 0$ and $\Delta T > 0$ will always result in $\Delta G < 0$, will always be spontaneous

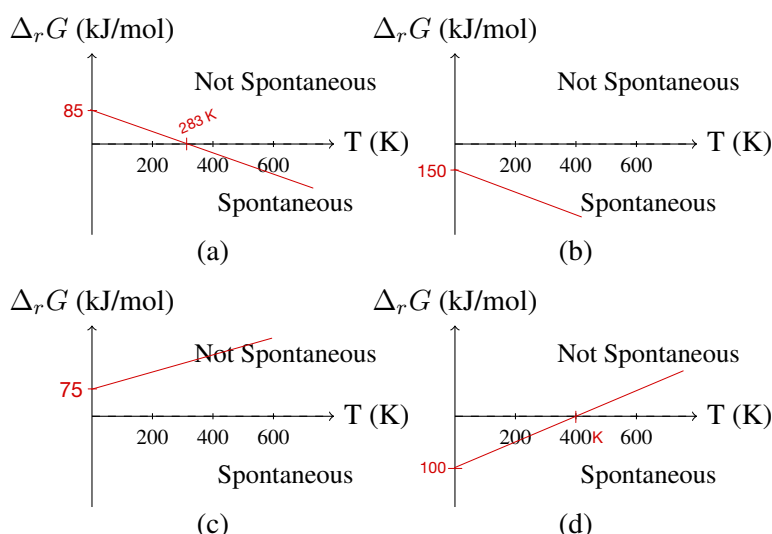
$$\Delta G = \Delta H - \Delta ST \rightarrow G = -150 * 10^3 - 200 * 298K \rightarrow G = -209.6 \text{ kJ/mol}$$

(c) $\Delta H > 0$ and $\Delta T < 0$ will always result in $\Delta G > 0$, will always be non-spontaneous

$$\Delta G = \Delta H - \Delta ST \rightarrow G = +75 * 10^3 - (-100) * 298K \rightarrow G = 104.8 \text{ kJ/mol}$$

(d) $\Delta H < 0$ and $\Delta T < 0$ will result in a shift for ΔG , will go from spontaneous to non-spontaneous at higher temperatures

$$\Delta G = \Delta H - \Delta ST \rightarrow 0 = -100 * 10^3 - (-250) * T \rightarrow T \approx 400K$$



Task 2: The reaction of 1 mole of Methane (CH_4) with 2 moles of air ($\text{O}_2 + 3.76\text{N}_2$) results in 1 mole of carbon dioxide (CO_2), 2 moles of water (H_2O) and 7.52 moles of (N_2). Calculate the mole and mass fraction of product species. Also, determine mole and mass fraction of air in the reactant mixture.

Atomic weights: C is 12.011 amu, H is 1 amu, O is 16 amu and N is 14 amu.

Answer: Total number of moles of product = $n_{\text{O}_2} + n_{\text{H}_2\text{O}} + n_{\text{N}_2}$

$$\sum X_i = 1 \text{ and } \sum Y_i = 1 \text{ for species } i = 1 \text{ to } n$$

Answer: We want to first calculate X_i and Y_i for all products and reactant air. We also perform a check of $\sum X_i = 1$ to ensure that the present amount of materials match up.

Product Calculations

$$X_i = \frac{n_i}{n_{tot,prod}} = n_{\text{CO}_2} + n_{\text{H}_2\text{O}} + n_{\text{N}_2} = 1 + 2 + 7.52 = 10.52 \text{ mol}$$

$$X_{\text{CO}_2} = \frac{1}{10.52} = 0.095 // X_{\text{H}_2\text{O}} = \frac{2}{10.52} = 0.190 // X_{\text{N}_2} = \frac{7.52}{10.52} = 0.715$$

$$\sum(X_i) = X_{\text{CO}_2} + X_{\text{H}_2\text{O}} + X_{\text{N}_2} = 1$$

Calculation of the total mass:

$$m_{tot} = W_{\text{CO}_2} * n_{\text{CO}_2} + W_{\text{H}_2\text{O}} * n_{\text{H}_2\text{O}} + W_{\text{N}_2} * n_{\text{N}_2} = 44.011 * 1 + 18 * 2 + 28 * 7.52 = 290.571 \text{ g}$$

Calculation of mass fractions:

$$Y = \frac{m_i}{m_{tot}} \rightarrow Y_{\text{CO}_2} = \frac{m_{\text{CO}_2}}{m_{tot}} = \frac{44.011}{290.571} = 0.151 // Y_{\text{H}_2\text{O}} = \frac{m_{\text{H}_2\text{O}}}{m_{tot}} = \frac{36}{290.571} = 0.124 // Y_{\text{N}_2} = \frac{m_{\text{N}_2}}{m_{tot}} = \frac{210.56}{290.571} = 0.725$$

Air Calculations

$$\sum(n_i) = n_{tot,rec} = n_{\text{CH}_4} + X_{air} = 1 + 2 = 3 \text{ mol}$$

$$X_{\text{CH}_4} = \frac{1}{3} = 0.33 // X_{air} = \frac{2}{3} = 0.66$$

Molecular weight is equal to the sum of all present atoms in the molecule. For methane the molecular weight is $W_{\text{CH}_4} = 12.011 * 1 + 4 * 1 = 16.011 \frac{\text{g}}{\text{mol}}$ and for air it's $W_{\text{air}} = \frac{1}{\frac{0.21}{32} + \frac{0.79}{28}} = 28.86 \frac{\text{g}}{\text{mol}}$

Calculation of the molecular weight of mixture:

$$m_{tot} = W_{\text{CH}_4} * x_{\text{CH}_4} + W_{\text{air}} * x_{\text{air}} = 44.011 * 0.33 + 28.86 * 0.66 = 33.57 \frac{\text{g}}{\text{mol}}$$

$$\text{Mass fraction of air in reactant mixture: } Y_{\text{air}} = \frac{X_{\text{air}} * W_{\text{air}}}{W_{\text{mix}}} = \frac{0.66 * 28.86}{33.57} = 0.567$$

Task 3: The piston of a vertical piston-cylinder device containing a gas has a mass of 60 kg and a cross-sectional area of 0.04 m^2 . The local atmospheric pressure is 0.97 bar. Furthermore, the piston is subjected to gravitational acceleration is 9.81 m/s^2 .

Hint: The Piston is frictionless.

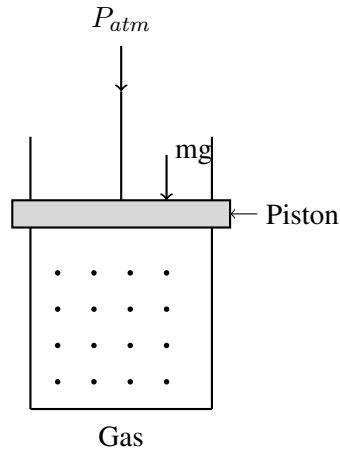


Figure 1: Vertical piston-cylinder device

(a) Determine the pressure inside the cylinder

To calculate the pressure inside the cylinder, we can use the fact that the pressure inside the cylinder must match the pressure exerted above the piston. The force balance equation from this situationen becomes the following

$$\begin{aligned} \text{Pressure inside column} &= \text{Pressure on column} \rightarrow p_{cylinder} * A = p_{atm} * A + m * g \\ p_{cylinder} &= p_{atm} + \frac{m * g}{A} = 0.97 * 10^5 + \frac{60 * 9.81}{0.04} = 111715[\text{pa}] = 1.12[\text{bar}] \end{aligned}$$

(b) If some heat is transferred to the gas, what will happen to the pressure and volume inside the cylinder?

When heat is introduced into the system, the gas will try to expand. Cause the piston is frictionless, it will move with the expansion, leading to an increase volume inside the cylinder. As long as the piston don't exert more force against the gas, the pressure will remain the same.

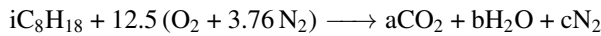
In summary, volume will increase and pressure will remain the same.

Exercise 2 - Thermochemistry

Herman Andersson
23th of July 2025

1. Task 1

Question: For a mixture of iso-octane (iC_8H_{18}) and air, the global reaction for complete combustion is given as



1. Determine a , b and c for the above reaction.
2. Calculate the mass-based air-to-fuel ratio for the above reaction.
3. Calculate the amount of air (in kg) required for complete combustion of 55.5 L (≈ 14.7 gallons) of iso-octane. 1 gallon = 2.7 kg

Consider Atomic weights: C is 12.011 amu, H is 1 amu, O is 16 amu and N is 14 amu

Answer 1: $iC_8H_{18} + 12.5(O_2 + 3.76N_2) \longrightarrow aCO_2 + bH_2O + cN_2$

As nitrogen is not consumed in the reation, we can read it from the air $c = 12.5 * 3.76 = 47 \rightarrow cN_2 = 47N_2$
 $a = 8$, cause iC_8H_{18} has all eight carbon atoms

$b = 9$, cause $\frac{18}{2} = 9$ for the hydrogen

Correct input for the global reaction in thus $iC_8H_{18} + 12.5(O_2 + 3.76N_2) \longrightarrow 8CO_2 + 9H_2O + 47N_2$

Answer 2: Calculations for molecular weight for air and fuel.

$$MW_{fuel} = 12.011 * 8 + 1 * 18 = 114.088 \frac{g}{mol} (\text{amu})$$

$$MW_{air} = \frac{1}{\frac{0.21}{32} + \frac{0.79}{28}} = 28.86 \frac{g}{mol} (\text{amu})$$

$$AFR = \frac{m_{air}}{m_{fuel}} = \frac{MW_{air} * n_{air}}{MW_{fuel} * n_{fuel}} = \frac{28.86 * 12.5}{114.088 * 1} = 3.16 \approx 3.2$$

Answer 3: $m_{fuel} = \rho * V = 2.7 \frac{kg}{gallon} * 14.7 \text{gallon} = 39.69 \text{kg}$

$$AFR = \frac{m_{air}}{m_{fuel}} \rightarrow m_{air} = AFR * m_{fuel} = 3.16 * 39.69 \text{kg} = 125.42 \text{kg}$$

2. Task 2

Question: For the combustion of iso-octane described in Task 1, calculate the equilibrium constant K_p at temperature $T=298$ K. Based on the obtained K_p value, comment on whether the reactant or product is favored during the reaction.

Supporting Information: $R = 8.314 \text{ J/mol K}$

$$\Delta G^0 = \sum (\Delta G_f^0 \text{ of products}) - \sum (\Delta G_f^0 \text{ of reactants}) \quad (1)$$

Substance/Species	$\Delta G_f^0 \text{ (kJ/mol)}$
C ₈ H ₁₈	-208.4
O ₂	0
CO ₂	-394.4
H ₂ O	-228.6
N ₂	0

Answer: Global reaction $i\text{C}_8\text{H}_{18} + 12.5(\text{O}_2 + 3.76\text{N}_2) \longrightarrow 8\text{CO}_2 + 9\text{H}_2\text{O} + 47\text{N}_2$

Gibbs energy from the reference table: $\Delta G^0 = (-394.4) + (-228.6) - (-208.4) = -414.6 \text{ kJ/mol}$

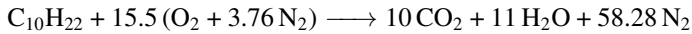
Calculating Equilibrium constant through Gibbs energy: $K_p = e^{\left(\frac{-\Delta G^0}{R \cdot T}\right)} = e^{\left(\frac{-(-414.6 \cdot 10^3)}{8.314 \cdot 298}\right)} = 4.7 \cdot 10^{72}$

Comments: If ΔG^0 is negative, it will cause $K_p > 1$, which is true in this case. If $K_p > 1$, it shows that the products will be favored.

The larger the $K_p = \text{value}$ is over one, the faster the reaction. Combustions are fast reactions, so we expect large K_p -values

3. Task 3

Question: For the complete combustion of gaseous n-decane ($C_{10}H_{22}$) in the air:



Determine the upper (HHV) and lower heating (LHV) values at 298 K of n-decane ($C_{10}H_{22}$) per kilogram of fuel. The molecular weight of n-decane is $142.284 \frac{kg}{kmol}$.

Supporting Information: Heat of vaporization of H_2O is 44010 kJ/kmol

Substance/Species	\hat{h}_f^0 (kJ/kmol) @ 298 K
$C_{10}H_{22}$	-249659
O_2	0
CO_2	-393546
H_2O	-241845
N_2	0

Answer: Standard enthalpy of combustion calculations ΔH_{comb}^0 : $\Delta H_{comb}^0 = \sum(\nu_i h_f^0 \text{ of products}) - \sum(\nu_i h_f^0 \text{ of reactants})$

$$= (10 \cdot h_f^0(CO_2) + 11 \cdot h_f^0(H_2O) + 58.28 \cdot h_f^0(N_2)) \\ - (1 \cdot h_f^0(C_{10}H_{22}) + 15.5 \cdot h_f^0(O_2) + 15.5 \cdot 3.76 \cdot h_f^0(N_2))$$

$$= (10 \cdot (-393546) + 11 \cdot (-241845) + 58.28 \cdot 0) - (1 \cdot (-249659) + 15.5 \cdot 0 + 58.28 \cdot 0)$$

$$= (-3935460 + (-2660295)) - (-249659) = -6346096 \frac{kJ}{kmol}$$

HHV can then be calculated with the molecular weight of the fuel.

$$M = 142.284 \frac{g}{mol} = 142.284 \frac{kg}{kmol}$$

$$HHV = \frac{|\Delta H_{comb}^0|}{M} = \frac{6346096}{142.284} = 44601.6 \frac{kJ}{kg}$$

HHV includes the total heat released during combustion, including the latent heat of vaporization of the water produced, which means that all the water vapor formed during combustion is condensed back to the liquid, releasing its latent heat. For LHV it is assumed that water vapor remains in the gaseous state and its latent heat is not recovered/released. So the difference between HHV and LHV is the heat of vaporization of water.

$$LHV = HHV - \frac{1}{M} \cdot n_{H_2O} \cdot h_{vap} = 44601.6 - \frac{11 \cdot 44010}{142.284} = 41199.2 \frac{kJ}{kg}$$

$$\text{Or in } \frac{kJ}{kmol} : LHV = 41199.2 \cdot 142.284 = 5861987 \frac{kJ}{kmol}$$

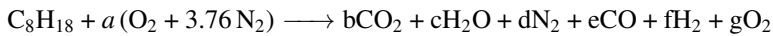
$HHV > LHV$ is expected. As stated above, HHV contains the latent heat of vaporization of water while LHV has used some of the energy to vaporize the water.

Exercise 3 - Reaction rates

Herman Andersson
23th of July 2025

1. Task 1

Question: For a mixture of iso-octane C₈H₁₈ and air, the global reaction for complete combustion is given as



1. Determine a, b, c, d, e, f and g for the stoichiometric mixture condition.

2. Calculate the equivalence ratio if the a in the global reaction above becomes $a + 2$. Is the mixture lean, rich or stoichiometric in this case?

Consider Atomic weights: C is 12.011 amu, H is 1 amu, O is 16 amu and N is 14 amu

Answer 1) Stoichiometric condition means that there is no excess of fuel or oxidizers. Meaning that there will only be the global products present (CO₂, H₂O and N₂) as no excess reactants forms unwanted byproducts. This will result in e, f, g equals zero. Meaning that the global reaction for stoichiometric conditions will look like
 $\text{C}_8\text{H}_{18} + a(\text{O}_2 + 3.76 \text{N}_2) \longrightarrow b\text{CO}_2 + c\text{H}_2\text{O} + d\text{N}_2$.

Setup of unknown variables

$$C : 8 = b + e$$

$$H : 18 = 2c + 2f$$

$$O : 2a = 2b + c + e + 2g$$

$$N : 7.52a = 2d$$

As e, f, g equals zero, we can perform the following calculations.

$$\begin{aligned} b &= 8, \text{ all carbon becomes CO}_2 \\ c &= \frac{18}{2} = 9 \text{ all hydrogen becomes H}_2 \\ 2a &= 2 \cdot 8 + 9 = 25 \Rightarrow a = \frac{25}{2} = 12.5 \\ d &= \frac{7.52a}{2} = \frac{7.52 \cdot 12.5}{2} = 47 \end{aligned}$$

Answer 2) In order to calculate if $a + 2$ becomes lean, rich or stoichiometric, we first need to calculate the Fuel to Air ratio (FAR) for both the stoichiometric condition and our changed condition.

$$FAR = \varphi = \frac{(fuel)}{(air)} \cdot \frac{(O_2)_{stoic}}{(fuel)_{stoic}}$$

$$\text{For our stoichiometric condition } FAR_{stoic} = \frac{(fuel)}{(air)}_{stoic} = \frac{8 \cdot 12.011 + 18 \cdot 1}{25 \cdot 16 \cdot 2} = \frac{114.088}{800} = 0.1426$$

$$\text{For our changed condition } FAR_{actual} = \frac{(fuel)}{(air)}_{actual} = \frac{8 \cdot 12.011 + 18 \cdot 1}{(25+2) \cdot 16 \cdot 2} = \frac{114.088}{864} = 0.1320$$

Equivalence ratio can then be calculated with equation 1.

$$\varphi = \frac{\left(\frac{Fuel}{Oxidizer}\right)_{actual}}{\left(\frac{Fuel}{Oxidizer}\right)_{stoichiometric}} \quad (1)$$

- $\varphi > 1 \Rightarrow$ Fuel rich mixture
- $\varphi < 1 \Rightarrow$ Fuel lean mixture
- $\varphi = 1 \Rightarrow$ Stoichiometric mixture

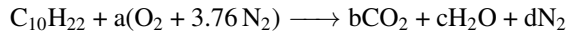
Which provide the equivalence value of $\varphi = \frac{O_2}{O_2+2} = \frac{0.1320}{0.1426} = 0.9259 < 1 \Rightarrow$ fuel lean solvent

2. Task 2

Question: Calculate constant-pressure adiabatic flame temperature for the combustion of a stoichiometric C₁₀H₂₂-air mixture. The pressure is 1 atm, and the initial reactant temperature is 298 K. Assume constant specific heats at product temperature. Enthalpy of formation and corresponding specific heating values for each species are available in the following table.

Species	\hat{h}_f^0 (kJ/kmol) @ 298 K	\hat{c}_p (kJ/kmol-K)
C ₁₀ H ₂₂	-249659	-
CO ₂	-393546	56.21
H ₂ O	-241845	43.87
N ₂	0	33.71
O ₂	0	-

The global reaction for stoichiometric C₁₀H₂₂-air mixture can be written as



As in Task 1, we can write the unknown variables for the global reaction and calculate the exact reactions for an balanced global reaction.

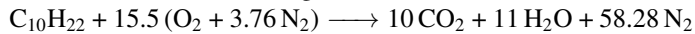
$$b = \text{number of C in fuel} \Rightarrow b = 10$$

$$c = \text{number of H in fuel} \Rightarrow c = 11$$

$$d = a \cdot 3.76$$

$$O : 2a = 2b + c = 2 \cdot 10 + 11 = 31 \Rightarrow a = 15.5$$

And thus the balanced global reaction can be written as



For the adiabatic flame temperature (AFT) calculation, we use the principles that all energy remains within the system and no heat is exchanged with the surroundings (adiabatic conditions). This means that the total enthalpy of reactants equals the total enthalpy of products. whereas excess energy from the enthalpy of formation goes to increasing the temperature of the products. Enthalpy of formation (\hat{h}_f^0) values represent the absolute enthalpy reference for each species at standard conditions (298 K). Meaning that the excess energy remaining after formation of products will be used to increase the temperature of the mixtures and thus provide the AFT. Pure elements, such as O₂ and N₂ in their standard states are references and thus have value of zero for \hat{h}_f^0 .

$$H_{react} = 1 \cdot (-249659) + 0 + 0 = (-249659) \text{ kJ/kmol}$$

$$H_{prod} = 10 \cdot (-393546) + c_{p,\text{CO}_2} \cdot (T_{ad} - 298) + 11 \cdot (-241845) + c_{p,\text{H}_2\text{O}} \cdot (T_{ad} - 298) +$$

$$58.28 \cdot (0 + c_{p,\text{N}_2} \cdot (T_{ad} - 298)) =$$

$$H_{react} = H_{prod} \Rightarrow T_{ad} = 2321.6 \text{ K}$$

3. Task 3

Question: Consider NO-formation reaction is executed through three elementary reactions, called the Zeldovich mechanism



Where, k_{1f} , k_{1r} , k_{2f} , k_{2r} , k_{3f} and k_{3r} are forward and reverse rate coefficients for each reaction.

Write the expression for the net rate of production of N_2 , O_2 , O , NO and N .

To determine the net rate of production for each species, we must consider all elementary reactions in which the species participates. The net rate equals the sum of production rates minus consumption rates across all reactions. For each species, we identify where it appears as a reactant (consumed, negative contribution) and as a product (produced, positive contribution). Each elementary reaction contributes terms proportional to the product of reactant concentrations multiplied by the respective rate constant. For reversible reactions, both forward and reverse directions must be included.

$$N_2 : \frac{dN_2}{dt} = -k_{1f}[N_2][O] + k_{1r}[NO][N]$$

$$O_2 : \frac{dO_2}{dt} = -k_{2f}[N][O_2] + k_{2r}[NO][O] - k_{3f}[O_2] + k_{3r}[O][O]$$

$$O : \frac{dO}{dt} = -k_{1f}[N_2][O] + k_{1r}[NO][N] + k_{2f}[N][O_2] - k_{2r}[NO][O] + 2 * (k_{3f}[O_2] - k_{3r}[O][O])$$

$$NO : \frac{dNO}{dt} = k_{1f}[N_2][O] - k_{1r}[NO][N] + k_{2f}[N][O_2] - k_{2r}[NO][O]$$

$$N : \frac{dN}{dt} = k_{1f}[N_2][O] - k_{1r}[NO][N] - k_{2f}[N][O_2] + k_{2r}[NO][O]$$

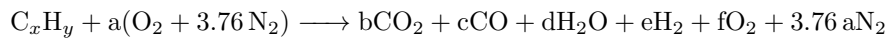
Exercise 4 - Adiabatic Flame Temperature for Methane

Herman Andersson
23th of July 2025

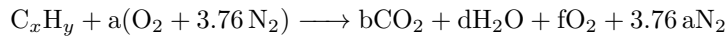
1. Problem 1.a - Combustion in Air

To calculate the temperature of the adiabatic flame (AFT) without using Cantera, we first define the combustion reaction of methane with air based on the global reaction and distinguish between lean-fuel ($\varphi \leq 1$) and rich-fuel ($\varphi > 1$) mixtures by using the equivalence ratio (φ). This allows us to identify the products and their amounts present after the combustion depending on the amount of oxygen reacted in the combustion.

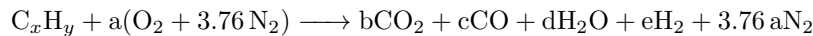
The global reaction for the combustion is:



For lean mixtures, we assume that not all oxygen has reacted, and thus the global reaction changes to have spare oxygen:



For the rich mixtures, we assume incomplete combustion. Due to the abundance in fuel, we get the following global reaction:



To compute the AFT, we apply the first law of thermodynamics for a steady-flow adiabatic system at constant pressure. This means the total enthalpy of reactants must equal the total enthalpy of products. The enthalpy of each species is calculated using its standard formation enthalpy at 298 K and then adjusted for temperature using temperature-dependent heat capacities ($C_p(T)$).

Because the product temperature (AFT) is unknown and appears inside integrals of $C_p(T)$, we use an iterative numerical approach. An initial temperature guess is refined until the enthalpy balance between reactants and products is satisfied within a small tolerance. This process is repeated across a range of equivalence ratios ($\varphi = 0.1$ to 2) to generate a curve of AFT versus φ . Figure 1 shows the results from the code run for combustion both in air and in pure oxygen for methane.

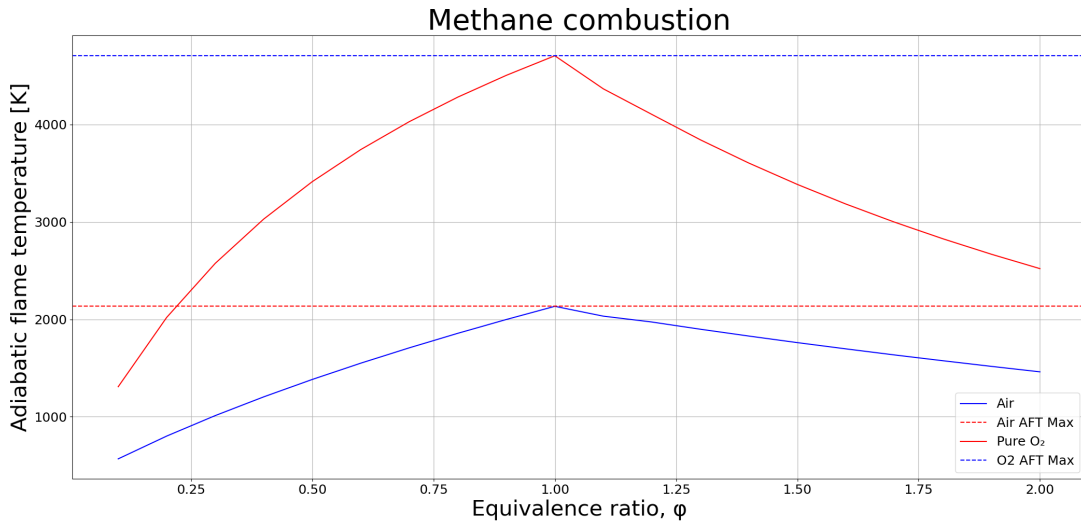


Figure 1: Adiabatic flame temperature vs. equivalence ratio for methane combustion in air and pure oxygen. Maximum AFT with air: 2134.08 K at $\phi = 1.00$. Maximum AFT with pure O₂: 4707.12 K at $\phi = 1.00$.

2. Problem 1.b - Combustion in pure oxygen

As we can see in the figure 1, the AFT for combustion in pure oxygen is significantly higher than combustion in air. This result was to be expected when looking at the global reaction. Nitrogen and oxygen have no enthalpy of formation when calculating the enthalpy of the reactants. So the overall energy in the combustion is still the same if the fuel is not changed. What is affected is the calculation for the enthalpy of the products, where one molecule, nitrogen, is removed from the equation. With nitrogen gone from the combustion, more of the energy goes to the molecules left and thus the AFT in the system becomes higher for combustion in pure oxygen than in air.

3. Problem 2 - Cantera Calculations

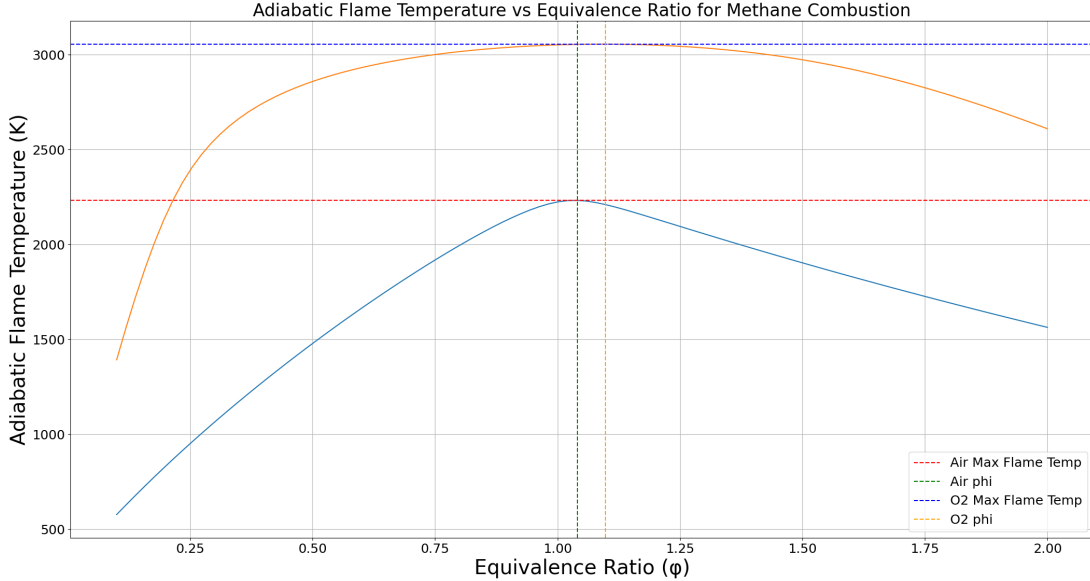


Figure 2: Max Adiabatic Flame Temperature with Air: 2232.66 K at Equivalence Ratio: 1.04,
Max Adiabatic Flame Temperature with pure O₂: 3055.85 K at Equivalence Ratio: 1.10,

When comparing the results from problem 1 with canteras calculation of the methane combustion we see differences at the AFT and φ values.

Table 1: Comparison of AFT results between Python and Cantera methods

Method	Case	AFT	φ
Python	Air	2134.08 K	1.00
Python	Oxygen	4707.12 K	1.00
Cantera	Air	2232.66 K	1.04
Cantera	Oxygen	3055.85 K	1.10

Canteras values for AFT are slightly lower in air combustion but greatly lower in oxygen combustion in comparison to problem 1. The equivalence ratio from problem 1 is also always one and the value from cantera are both slightly higher than one.

The reasoning for these differences comes down to several factors.

First the Dissociation effects

Dissociation effects refers to the breakdown of combustion products such as CO₂ and H₂O into their constituent atoms or molecules when exposed to high temperatures which may be reached during combustions. These reactions often require energy to break the molecular bonds, which otherwise would have gone to increasing the temperature in the combustion and thus resulted in a higher AFT.

In problem 1, these dissociation effects are ignored and only focuses on the global reactions products such as H₂O, CO₂ and in cases of rich mixtures, H₂ and CO.

Cantera's gri30.yaml file which has over 300 reactions covers several different reactions between all present molecules in the global reaction setup, where some reactions present the dissociation effects.

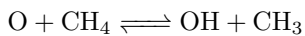
Difference in the amount of Thermodynamic Data available

In problem 1, the data present is Standard enthalpy of formation, $C_{p,i}$ at 1200 kelvin, Water-gas equilibrium and the coefficients for calculating C_p in the interval between 1000-5000 kelvin. Gri30.yaml itself consists of 1778 lines of code, where a large part is just thermodynamic data. For example, Cantera has data to accurately calculate the C_p -value for all 53 species present in gri30 with temperatures interval between 200-1000K and 1000-3500K or 200-1000K and 1000-6000K.

Simplified Reactions

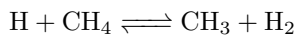
Problem 1 only assumes the global reaction takes place, with the expectation of Water-Gas equilibrium reaction $\text{CO} + \text{H}_2\text{O} \longleftrightarrow \text{CO}_2 + \text{H}_2$ in fuel rich mixtures. The global reaction is also not a reversible reaction due to its simplicity and how unlikely the reaction is to occur backwards.

Cantera on the other hand handles several more reactions, which is also reversible due to being single step elementary reactions. For example Reaction 11 which shows that methane could react with oxygen at the start of the combustion.

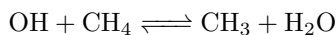


(Reaction 11)

We could also look at reaction 53 and 98 to see how methane reacts with potential bi-products from the combustion after initialization.



(Reaction 53)



(Reaction 98)

So to summarize, Cantera shows different AFT-values than problem 1 due to cantera calculating the elementary reactions that take place instead of just the global reaction that problem 1 handles. This is also the reason why φ is one in problem 1 and slightly higher in cantera. Problem 1 calculation is the stoichiometric peak which occurs when $\varphi = 1$. Cantera requires a slightly higher φ value to ensure the fuel is fully combusted and the maximum of energy released.

Exercise 5 - Prediction of NO concentration at varying equivalence ratio

Herman Andersson
23th of July 2025

1. Introduction & Problem

Nitrogen oxides (NO_x), comprising nitric oxide (NO) and nitrogen dioxide (NO_2), are gases produced by natural sources, vehicles, and fuel-burning processes. While NO is colorless, it oxidizes in the atmosphere to form NO_2 , an odorous, corrosive gas that contributes to photochemical smog and poses significant health and environmental risks. High NO_2 levels can damage the respiratory system, worsen asthma, impair senses, and harm vegetation and materials. Air quality standards from Queensland's government were set to a limit for NO_2 to 0.08 ppm over 1 hour and 0.015 ppm annually.

In hydrocarbon combustion, such as methane-air systems, NO formation is highly temperature-dependent and varies with operating conditions like the equivalence ratio (φ). So the interest to study the equivalence ratio effects on NO is of great importance to reduce pollution in the atmosphere. NO can also be produced by nitrogen bounded fuels where the present nitrogen gets oxidized to NO and flame generated NO which only occurs in the flame front due to intermediate combustion species.

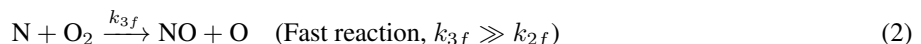
2. Theory and Method

2.1 Assumptions

For this assignment, we assume the following to simplify the calculations:

- First we assume that NO is formed considering simple Zeldovich Mechanism (see equations 1 and 2).

Zeldovich or thermal mechanism for the formation of NO from atmospheric N_2 :



- $[\text{N}]$ is assumed to be in Quasi Steady State (QSSA). QSSA is a state where the change in certain species concentrations is considered negligible compared to the overall reaction rate.

- O_2 and 2O are assumed to be in equilibrium (applicable for high temperature system) (see equation 3):



- Reverse reaction rates in Zeldovich Mechanism are negligible as compared to forward reaction rates. Thus we will only calculate the forward reaction rate (k_{2f} and k_{3f}) and will ignore the backwards reaction rate (k_{2r} and k_{3r}).

We will also assume that the equivalence ratio (φ) varies between 0.6 to 2. The initial reactant temperature is 298 K and assume constant pressure of 101325 Pa. The initial mole fractions for nitrogen (X_{N_2}) is 0.79 and for oxygen (X_{O_2}) is 0.21. The initial reactant temperature is 298 K and the residence time (t) for the reaction is 5 ms.

2.2 Calculations

In order to calculate the nitrogen oxide formation, we need the setup of the reaction rate and formation per time unit. From the global reaction of nitrogen oxide formation (equation 4), we can get the rate law for the global reaction, see equation 5.



$$\frac{d[NO]}{dt} = k_G [N_2]^m [O_2]^n \quad (5)$$

Zeldovich mechanism, which explains the thermal formation of NO during high-temperature combustion. It involves two main reactions: nitrogen (N_2) reacts with atomic oxygen (O) to form nitric oxide (NO) and nitrogen atoms (N), followed by the rapid reaction of N with molecular oxygen (O_2) to form more NO and O . The first step is the rate-determining reaction, due to the second reaction occurring much faster ($k_{3f} \gg k_{2f}$). From this reaction we can get the reaction rate for the formation of NO and N , see equations 6 and 7.

$$\frac{d[NO]}{dt} = k_{2f} [N_2] [O] + k_{3f} [N] [O_2] \quad (6)$$

$$\frac{d[N]}{dt} = k_{2f} [N_2] [O] - k_{3f} [N] [O_2] \quad (7)$$

Where the reaction rate coefficient can be calculated from equations 8 and 9:

$$k_{2f} = 1.8 \times 10^{14} \exp\left(\frac{-318000}{RT}\right) \frac{\text{cm}^3}{\text{mol} \cdot \text{s}} \quad (8)$$

$$k_{3f} = 9.0 \times 10^9 \exp\left(\frac{-27000}{RT}\right) \text{cm}^3 / (\text{mol} \cdot \text{s}) \quad (9)$$

Nitrogen can be assumed to be in a QSSA state as its reaction is almost instantaneous and is consumed as fast as it is produced. From the QSSA assumption, we can derive equation 10 which with substitution in equation 6 will provide equation 11.

$$[N]_{ss} = \frac{k_{2f} [N_2] [O]}{k_{3f} [O_2]} \quad (10)$$

$$\frac{d[NO]}{dt} = 2k_{2f} [N_2] [O] \quad (11)$$

We calculate the concentration of single oxygen through rearranging the standard equilibrium formula based on our previous assumption. That for any reaction $aA + bB \rightleftharpoons cC + dD$ in equilibrium can be written as (equilibrium equation):

$$K_p = \frac{\left(\frac{P_C}{P^0}\right)^c \left(\frac{P_D}{P^0}\right)^d}{\left(\frac{P_A}{P^0}\right)^a \left(\frac{P_B}{P^0}\right)^b} \quad (12)$$

And in our case, be rewritten as equation 13 using equation 3 as reference.

$$[O] = [O_2] \left[\frac{K_p P^0}{R_u T} \right]^{1/2} \quad (13)$$

The equilibrium constant can be calculated using the equilibrium equation 14. The theta values are calculated from ($\theta = T/1000$) and the alpha values are, $a_1 = 6.434$, $a_2 = -0.2755$, $a_3 = 0.02396$, $a_4 = -0.111 \times 10^{-2}$, $a_5 = 0.8258$, $a_6 = -25.80$

$$\log_{10} K_p = a_1 + a_2 \theta + a_3 \theta^2 + a_4 \theta^3 + a_5 \ln(\theta) + \frac{a_6}{\theta} \quad (14)$$

Substituting equation 13 in equation 11 will give equation 15.

$$\frac{d[NO]}{dt} = 2k_{2f} \left(\frac{K_p P^0}{R_u T} \right)^{1/2} [N_2][O_2]^{1/2} \quad (15)$$

If we take into account the average time the reactants spend in the high-temperature combustion zone where the reaction takes place, we get the final equation to calculate the concentration of nitrogen oxide, see equation 16.

$$[NO] = \frac{d[NO]}{dt} \times \text{residence time} \quad (16)$$

Comparing the rate of formation reaction for nitrogen oxide (eq 15) with the rate law for the global reaction (eq 5), we can get the values for the overall reaction coefficient K_G through equation 17 and the exponential values $m = 1$ and $n = 1/2$ for the rate law for the global reaction.

$$k_G = 2k_{2f} \left(\frac{K_p P^0}{R_u T} \right)^{1/2}, m = 1 \text{ and } n = 1/2 \quad (17)$$

3. Results

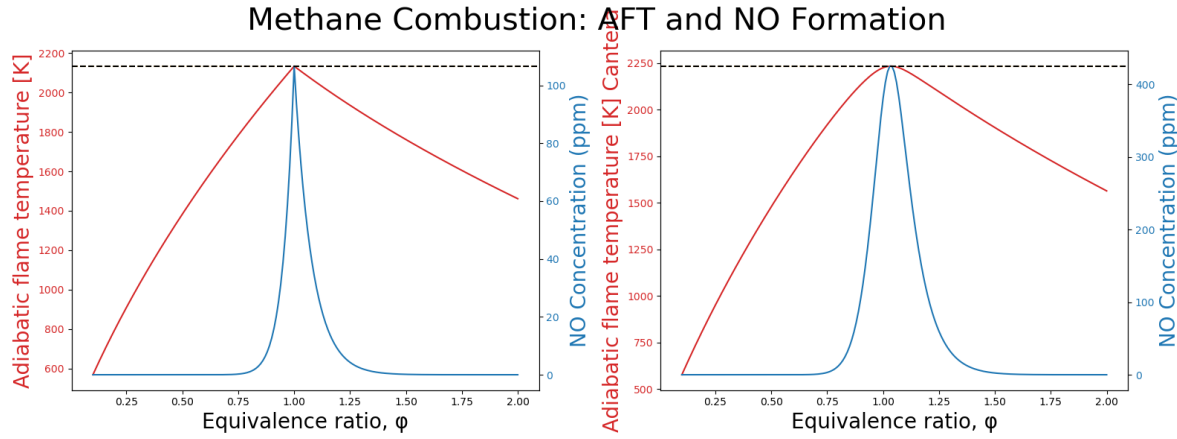


Figure 1: The red lines represent the adiabatic flame temperature in kelvin calculated from the previous task and the blue lines represent the concentration of NO in parts per million against the equivalence ratio. The left figure shows the calculations made through python and the right figure shows the values calculated with the Cantera software.

Table 1: Maximum Values and Corresponding Equivalence Ratios

Parameter	Max Value	at $\varphi =$
Max temp for Python (K)	2134.08	1.000
Max temp for Cantera (K)	2232.72	1.030
Max NO ppm for Python	106.60	1.000
Max NO ppm for Cantera	425.16	1.030

4. Discussion and Conclusion

From figure 1 we see that the NO is mainly formed when the equivalence ratio φ is between 0.8-1.30, where the AFT values differ between roughly 1850K and 1900K for python calculations. With a maximum at the same φ value as the maximum AFT temp.

This is expected as our calculations are based on the Zeldovich mechanism which is founded on the dissociation of N₂ in air at temperatures beyond 1850K. To achieve this temperature, there needs to be an optimal balance of oxygen and fuel present. Low φ values (lean conditions) provide excess oxygen but insufficient fuel, resulting in lower combustion temperatures due to the heat sink effect of excess air and incomplete fuel utilization. Conversely, high φ values (rich conditions) provide excess fuel but insufficient oxygen for complete combustion, which reduces flame temperatures as more fuel gets heated up without fully reacting to release all available chemical energy. The optimal φ range of 0.8-1.3 achieves the necessary high temperatures (>1850K) and provides sufficient oxygen atoms for the Zeldovich mechanism reactions, with peak NO formation occurring near stoichiometric conditions where combustion efficiency and temperature are maximized.

The difference in NO concentration between Cantera and python is likely due to the calculations steps and chemical reactions that differ between the two methods. Python's calculation steps are described above under Calculation while Canteras steps are far more sophisticated and detailed. We only take into consideration the Zeldovich mechanism for the NO formation while cantera also takes into account several other present elementary reactions and intermediate pathways.

So to summarize, the formation rate of nitric acids is directly related to the equivalence ratio through the different adiabatic flame temperatures generated through the methane-air combustion. We can also conclude that φ affects the formation of nitric acids in other ways than just Zeldovich mechanism from comparing the values between python and Cantera, where cantera has almost four times higher concentration of nitric acids than the python calculations.

Exercise 6 - Determination of ignition delay time of methane-air mixture using Cantera

Herman Andersson
23th of July 2025

1. Introduction & Problem

Ignition delay refers to the time interval between the injection of fuel and the onset of combustion in an internal combustion engine. During this period, the injected fuel mixes with hot, compressed air and vaporizes. Once sufficient mixing and vaporization occur, spontaneous ignition takes place, initiating the combustion process.

The duration of ignition delay plays a crucial role in engine performance and emissions. A longer ignition delay allows more fuel to accumulate and vaporize within the combustion chamber, often resulting in a sudden and intense combustion event. This rapid combustion can generate high-pressure shock waves and extremely elevated surface temperatures, which may contribute to mechanical stress on engine components. Prolonged ignition delays are associated with increased loading on the piston crown, potential breakage of piston rings, and material degradation due to erosion caused by hot gas flow.

Moreover, the elevated temperatures resulting from extended ignition delay can lead to higher emissions of nitrogen oxides (NO_x), a major environmental pollutant. Understanding and accurately predicting ignition delay is therefore essential for optimizing engine design, improving fuel efficiency, and controlling emissions.

This report focuses on analyzing ignition delay as a factor of equivalence ratio, temperature and pressure and comparing it to experimental data so see the accuracy of the model.

2. Theory and Method

IDT is experimentally determined using two primary experimental facilities, each designed for different temperature regimes. Rapid Compression Machines (RCM) are employed for low-temperature studies (typically 600-1000K), where the fuel-air mixture is compressed adiabatically to achieve the desired thermodynamic conditions. The compression process heats the mixture to ignition temperatures while maintaining controlled temperature histories. Shock Tubes are utilized for high-temperature investigations (1000-2500K and above), where reflected shock waves instantaneously heat the test mixture to the target conditions. The shock tube provides precise control over initial temperature and pressure while eliminating gradual heating effects that could influence the ignition process.

IDT determination uses a zero-dimensional (0D) reactor model, which assumes the system has a uniform thermodynamic state everywhere. This means there are no spatial differences or transport effects, so the complex equations are simplified to ordinary differential equations. As temperature, species concentration and pressure/volume (depending on reactor model) changes due to chemical reactions taking place during the ignition, changes in time can be observed and collected for future analysis.

Figure 1 illustrates the pressure and species changes that take place during a shock tube experiment. The incident shock is when the pressure rise in the driver gets high enough to break the diaphragm. When the incident shock reaches the end

of the tube and gets reflected, this results in a pressure increase called the reflected shock. The reflected shock provides the energy required to start the chemical reaction and ignition. Initially, this compression creates a relatively stable environment where slow induction chemistry dominates, with chain-branching reactions gradually building up radical while competing with termination processes until the ignition points which results in a rapid pressure rise. Thus when calculating IDT, when the reflected shock reaches its maximum pressure is often used as the time point zero for IDT calculations.

There are several definitions for IDT and methods to calculate the point of ignition. They are based on the different parameters observed in the shock tube. It can be calculated between the reflected shock and when the pressure rises from chemical reactions (bottom of ignition in figure 1), or from temperature jumps due to exothermic reactions. It can also be calculated from the peaks of selected radical species, such as OH, CH, OH*, and CH* seen in figure 1, or by tracking rapid fuel consumption. Additional methods include direct visualization using high-speed cameras to detect chemiluminescence ($\lambda_{OH^*} = 308$ nm and $\lambda_{CH^*} = 430$ nm) and flame appearance. Cantera uses the species concentration method and defines the IDT at specified ground-state species peak concentration.

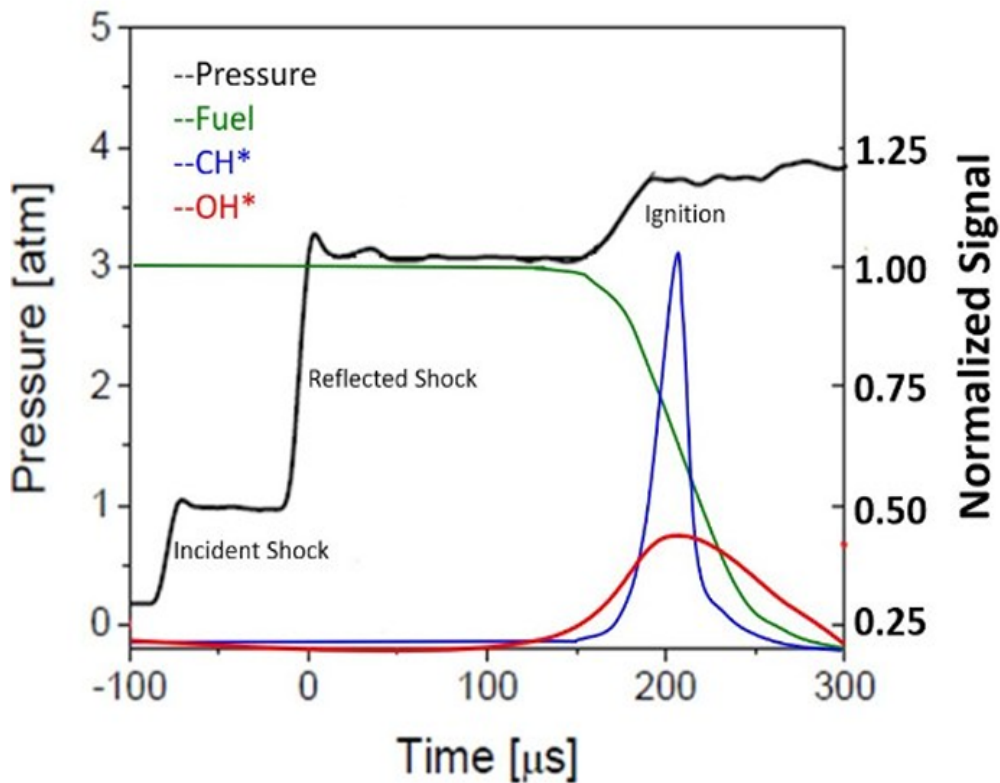


Figure 1: Pressure and species concentration changes over time for a shock tube experiment. The black line represents the pressure changes inside the shock tube. Split into different shock sections that occur during the experiment. Green, blue and red represent different species normalized concentration signals (between 0-1).

3. Results

Three cases for ignition delay time were calculated and compared to experimental results. All cases calculated the IDT in the temperature range of 800-2000K with different equivalence values of 0.5 for case one, 1.0 for case two and 2.0 for case three. The initial pressure varied between 1, 3, 5, 10, 25 and 44 atm, see figures 2 to 4. Table 1 presents the ignition delay time for all three cases at the point where the temperature fulfills the condition of $1000/T = 0.55$.

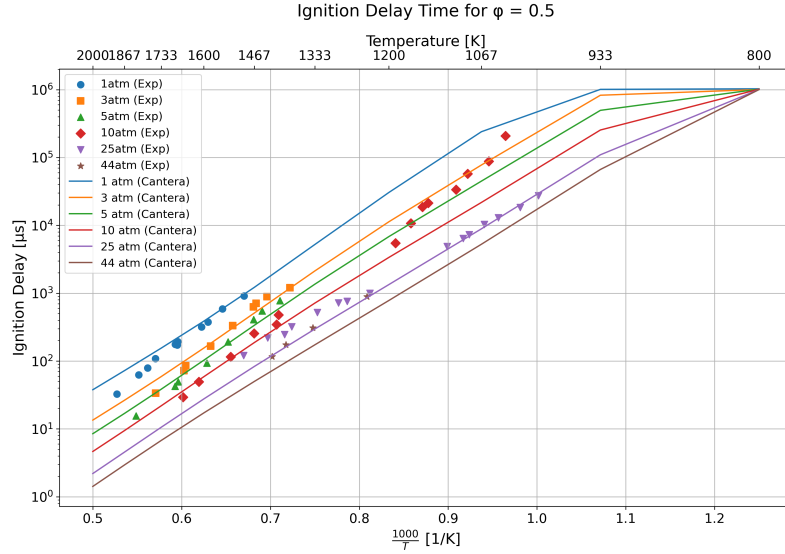


Figure 2: Cantera calculations for Ignition delay time compared with experimental data with equivalence ratio of 0.5 against the inverse logarithm of temperature. Lines represent canteras calculated values and markers represent experimental data.

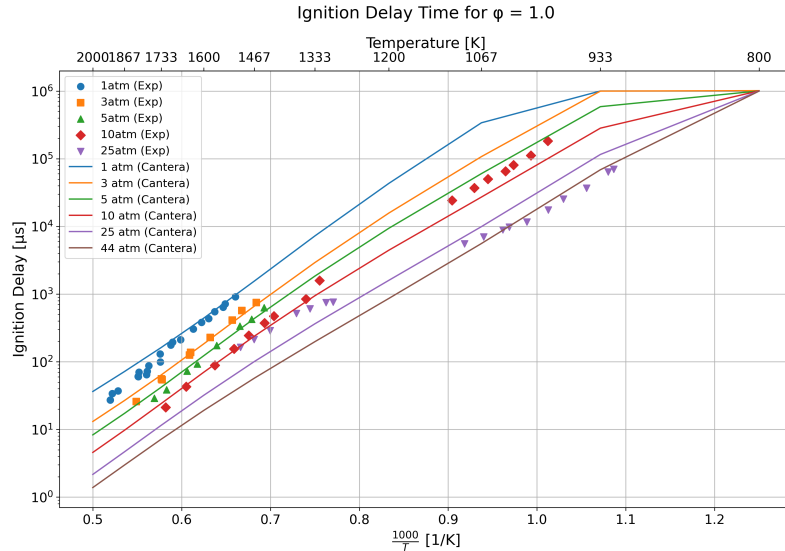


Figure 3: Cantera calculations for Ignition delay time compared with experimental data with equivalence ratio of 1.0 against the inverse logarithm of temperature. Lines represent canteras calculated values and markers represent experimental data.

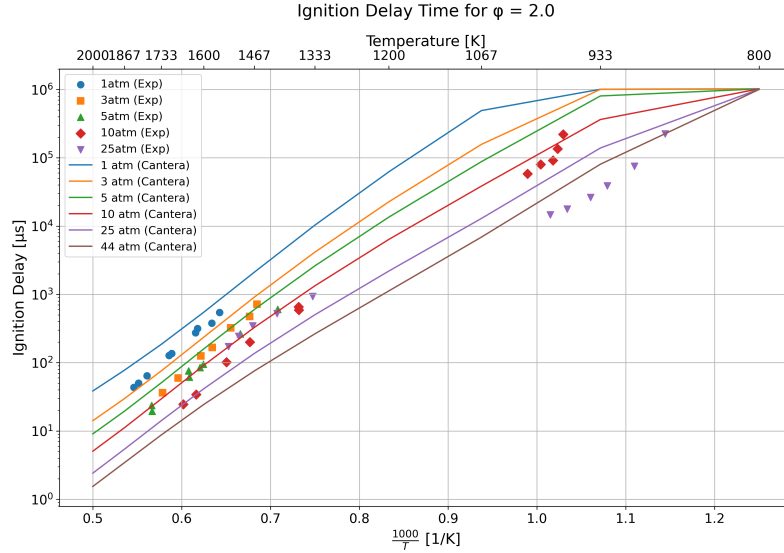


Figure 4: Cantera calculations for Ignition delay time compared with experimental data with equivalence ratio of 2.0 against the inverse logarithm of temperature. Lines represent canteras calculated values and markers represent experimental data.

Table 1: Ignition delay time [μs] at $1000/T = 0.55$ at varying pressures and equivalence ratios

φ	1 atm	3 atm	5 atm	10 atm
0.5	118.46 [μs]	44.40 [μs]	28.75 [μs]	16.28 [μs]
1.0	121.51 [μs]	46.82 [μs]	30.66 [μs]	17.51 [μs]
2.0	135.54 [μs]	54.16 [μs]	36.00 [μs]	20.88 [μs]

4. Discussion and Conclusion

First to note is the plateau seen when the IDT reaches 1s. This is an numerical error from the script generating the plots as the estimated IDT value is set to 1s and works as a hard upper limit in the calculations. As our experimental data doesn't go over this value, this error can for the present be ignored but would need to be fixed for calculations and simulations of lower temperature environments.

From the results we can observe three different effects caused by the changes of equivalence ratio, pressure and temperature.

4.1 Effect of Temperature on IDT

We see that for all equivalence ratios and pressures, an increase in temperature results in a decrease in IDT. This behaviour follows Arrhenius kinetics as higher temperatures both result in more energy in the system, allowing for more chain-branching reactions to pass the activation energy barrier as well as a higher temperature results in faster reaction rates.

4.2 Effect of Pressure on IDT

Pressure difference shows a consistent pattern across all equivalence ratios, with higher pressures leading to shorter IDT. This is most likely due to a higher pressure resulting in an increased molecular density. At elevated pressures, molecules are compressed into a smaller volume resulting in an increase in collision frequency which increases the overall reaction rates.

4.3 Effect of Equivalence Ratio (φ) on IDT

Equivalence ratio effects show distinct patterns with $\varphi = 0.5$ producing the shortest IDT values, followed by $\varphi = 1.0$, and $\varphi = 2.0$ showing the longest delays, see table 1 for reference. This occurs because lean conditions provide abundant oxygen for efficient chain-branching reactions, with the excess oxidizer effect overcoming fuel dilution and pushing the equilibrium towards the radicals. Rich mixtures suffer from oxygen limitation, forcing slower alternative reaction pathways that require higher thermal energy to achieve ignition.

We also observe a slope variation, with rich mixtures exhibit the steepest slope, then stoichiometric mixture and lean mixture the most gentle slope. This shows that rich mixtures are more temperature sensitive, with a small change in temperature resulting in a larger difference of IDT. This occurs because different mixture compositions promote distinct reaction pathways with varying activation energy requirements, effectively changing the overall energy barrier as a weighted combination of all active pathways.

4.4 Cantera vs Experimental Data

The comparison between Cantera simulations and experimental data demonstrates good fitting and accuracy for lean and stoichiometric conditions ($\varphi = 0.5$ and 1.0) for high temperturs ($T > 1400\text{K}$) and pressures below 10 atm. However, some deviation is observed for rich conditions ($\varphi = 2.0$) and pressure 25 respectively 44 atm. These deviations may occur for various reasons. One might be that the method of calculating IDT is varying. The IDT values may vary up to 10% depending on the definition and method for calculating the IDT values. However, this is an unlikely cause due to the fitting of the lean and stoichiometric conditions.

Another possibility is that the GRI-3.0 mechanism has limitations under rich and high pressure combustion conditions. While GRI is designed for $\varphi = 0.1 - 5$, most experimental data is around $\varphi = 1$, so it misses important information/parameters for higher ratios, leading to incorrect radical formation and difference between Cantera and experimental

data. GRI-3.0 is also designed for temperature intervals between 1000-2500K and pressure ranges between 10 Torr (0.013158 atm) to 10 atm. This would explain why our Cantera calculations and experimental data doesn't match for pressures above 10 atm, which we can see in figures 2 to 4 where 25 atm and 44 atm is inconsistent with experimental data.

The unique behavior of experimental data for 10 atm at $\varphi = 0.5$ for lower temperatures in figure 2 stands out from the rest IDT-values. As these conditions are within the pressure range and temperature range of GRI-3.0 and the model would need to cross over the IDT-values of lower pressures to fit the data. The likely cause for this inconsistency is experimental errors during experimental data collection.

Exercise 7 - Determination of laminar flame speed of premixed methane-air mixture

Herman Andersson
23th of July 2025

1. Introduction & Problem

Flame speed is the measure of the rate of expansion of a flame front in a combustion reaction. It can also be defined as the rate at which the unburnt mixture enters the flame. There are two primary types of flame speeds, laminar flame speed and turbulent flame speed. Laminar flame speed refers to the speed of a flame front propagating through a uniform, un-turbulent mixture. On the other hand, turbulent flame speed contains turbulence, which causes the flame front to behave irregularly such as swirling and eddies.

Accurate determination of flame speed is critical for several applications, including internal combustion engine design, optimization of combustion performance, development of predictive combustion models, and ensuring fire safety and explosion prevention. Additionally, flame speed measurements serve as a valuable tool for validating chemical kinetic mechanisms that describe complex combustion processes. By comparing computational predictions with experimental results, these mechanisms can be evaluated and refined for improved accuracy.

This report focuses on determining the laminar flame speed of a premixed methane-air mixture using numerical methods through Cantera and comparing the results with experimental data. We will examine two cases: the effect of varying initial pressure at constant temperature, and the effect of varying unburned mixture temperature at constant pressure, across an equivalence ratio range of 0.5 to 1.5.

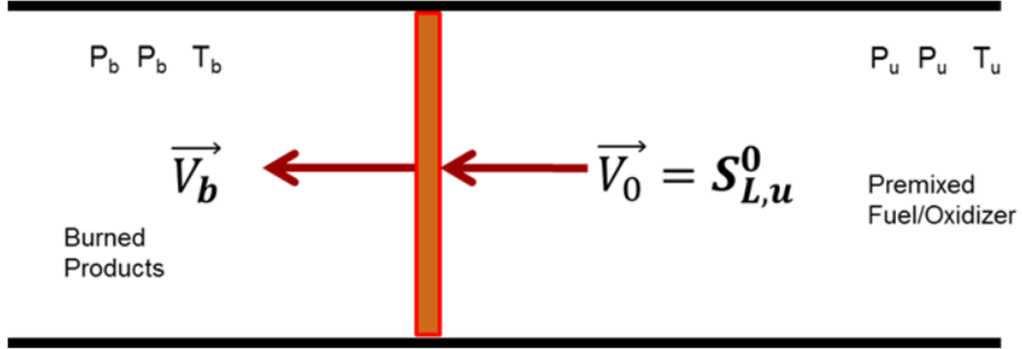
2. Theory and Method

When calculating flame speed, one either chooses to keep the flame front stationary and move the fuel through the flame front or vice versa. In this report, we have chosen to go with the second approach and keep the liquids stationary. Cantera also offers several models to represent the reactive flows. They are:

- Freely propagating premixed flames (chosen model in this report)
- Burner stabilized premixed flames
- Counterflow (strained) premixed flames

Freely propagating premixed flames are flames where the fuel and oxidizer are mixed before ignition and the flame front propagates through the mixture without being stabilized by a burner or other solid structure. Burner stabilized premixed flames are the same with the difference that it's anchored to a boundary instead of being freely propagating.

Counterflow (strained) flames are a type of flame where the premixed fuel and oxidizer is forced to flow against a flow of hot combustion products or an inert gas, creating a stagnation point.



Freely propagating flame

Figure 1: Red illustrates the flame front. Left side is burned reacted products and the right side is the premixed fuel and oxidizer. Red arrows illustrate the path the fuel and oxidizer moves through the flame front.

Appropriate boundary conditions are essential to ensure reliable and meaningful results. For 1D reaction flow simulations, such as freely propagating premixed flames, Danckwerts boundary conditions can be applied.

Danckwerts boundary conditions are a set of conditions used to describe the behavior of concentration profiles at the inlet and outlet of a reactor. It's used when high reaction rates are anticipated near the inlet and calculates the flux of species across the boundaries instead of specifying the concentrations, see equation 1&2

$$\text{Inlet } (x = 0) \begin{cases} T = T_0 \\ \rho u \omega_k + \rho \omega_k V_k = (\rho u \omega)_0 \quad k = 1, \dots, N_S \end{cases} \quad (1)$$

$$\text{Outlet } (x = L) \begin{cases} \frac{dT}{dx} = 0 \\ \frac{d\omega_k}{dx} = 0 \quad k = 1, \dots, N_S \end{cases} \quad (2)$$

Because the mass flow rate of the mixture is a part of the solution, an additional constraint, temperature, is required. The temperature value is fixed at a specific x-value to ensure that the gradient at the inlet remains zero in order to prevent heat loss, see equation 3.

$$\begin{cases} \frac{dm}{dx} = 0 \\ T(x = x_{fixed}) = T_{fixed} \end{cases} \quad (3)$$

Where $\frac{dm}{dx} = 0$ ensures that there is no mass flux and $T(x=x_{fixed}) = T_{fixed}$ gives the specific coordinate the required temperature to fulfill the conditions.

Cantera's calculations of the flame speed follows the thermal theory of Mallard-Le Chatelier. The Mallard-Le Chatelier theory views flame propagation as a process of heat transfer. The heat conducted from the burning zone is equal to the heat required to raise the premixed mixtures temperature to the ignition temperature, from T_0 to $T_{ignition}$, see figure 2.

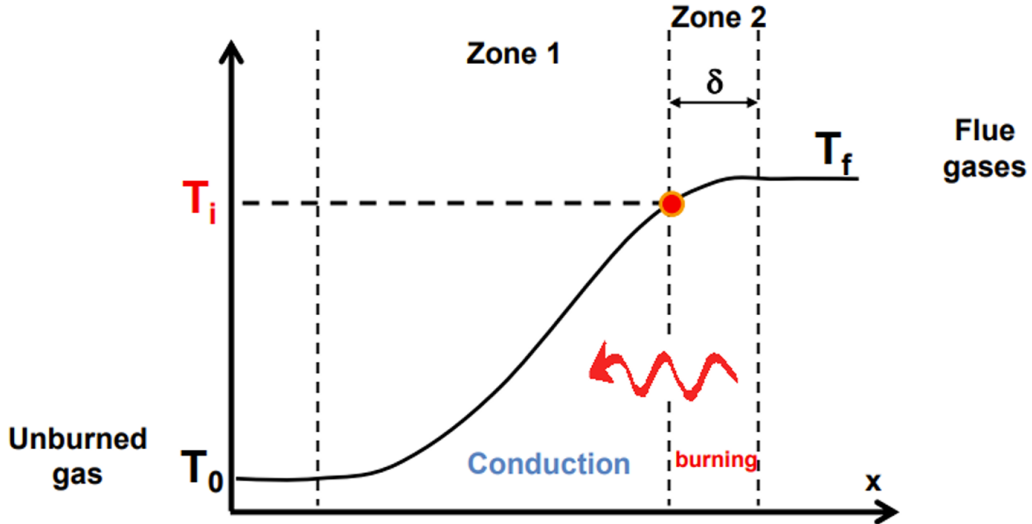


Figure 2: Visual illustration of Mallard-Le Chatelier thermal theory. T_0 equal the initial unburned temperature, T_f is the flue gases exiting temperature. Zone 1 represents the unignited mixture and zone 2 represents the burning zone where the mixture has been ignited. T_i represents the ignition temperature when crossing from zone 1 to zone 2.

By approximating the slope of the profile presented in figure 2 linearly, the enthalpy balance can be written as an equation 4 & 5. Where λ is the thermal conductivity, \dot{m} is the mass flow rate per unit area, ρ is the unburned gas density and δ is the flame thickness. S_L is laminar flame speed, c_p specific heat capacity and T_0 , T_i and T_f represent the initial-, ignition- and final temperature (AFT).

$$\dot{m}c_p(T_i - T_0) = \lambda(T_f - T_i)/\delta \quad (4)$$

$$\dot{m} = \rho \cdot S_L \quad (5)$$

3. Results

Two cases for laminar flame speed were calculated and compared to experimental results. Both cases calculated the laminar flame speed in the equivalence ratio range of 0.5-1.5.

Case 1 was calculated with an constant unburnt mixture temperature of 298 K with varying initial pressure at 1, 2, 5 and 20 atm, see figure 3.

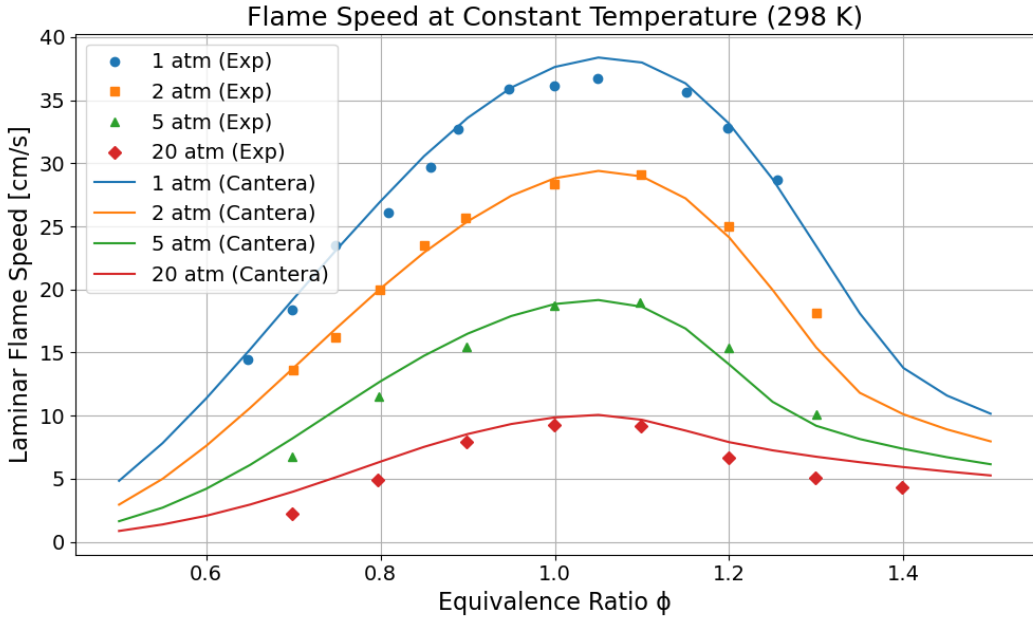


Figure 3: Cantera calculations for laminar flame speed against experimental data with constant temperature. Lines represent Cantera's calculated values and markers represent experimental data.

Case 2 was calculated with a constant initial pressure of 1 atm and with varying unburnt mixture temperatures of 358 K, 393 K and 428 K, see figure 4.

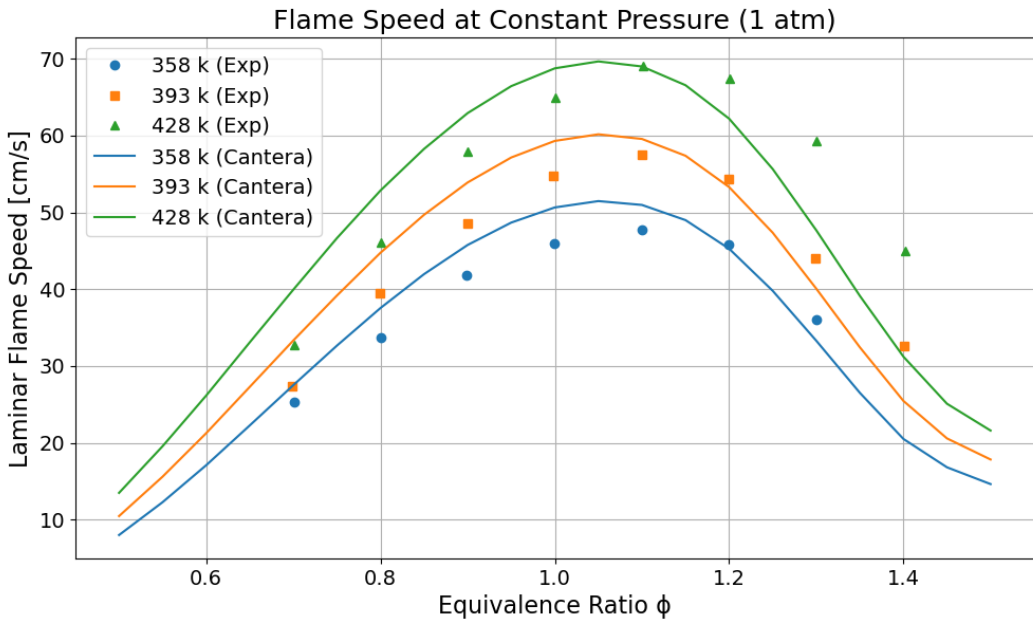


Figure 4: Cantera calculations for laminar flame speed against experimental data with constant pressure. Lines represent Cantera's calculated values and markers represent experimental data.

4. Discussion and Conclusion

For both cases, the maximum laminar flame speed is near stoichiometric conditions, between equivalence ratio 1~1.1. This is consistent with other experiments that show the fuel and oxidizer are optimally balanced for complete combustion and maximal heat release within this range.

We see in Figure 3 that at constant temperature, increasing pressure leads to a decrease in laminar flame speed. This is likely because higher pressure shifts the reaction equilibrium toward radical termination reactions, such as $\text{CH}_4 \rightleftharpoons \text{CH}_3 + \text{H}^*$, favoring the reverse direction. The increased collisional frequency at higher pressures enhances three-body recombination and termination reactions, reducing the concentration of key radicals like H, O, and OH that are essential for sustaining flame propagation. The higher pressure also increases the density of the unburned gas mixture. Limiting the ability of heat and reactive radicals to diffuse ahead of the flame front.

In figure 4, we see that at constant pressure, increasing temperature leads to an increase in laminar flame speed. An increase in initial temperature results in an increase in adiabatic flame temperature for the whole combustion. According to the Arrhenius equation, the reaction rate is proportional to the temperature, so a higher temperature leads to a higher reaction rate which increases the flame speed as more energy is released in a shorter amount of time.

The higher temperature also leads to a higher thermal diffusivity, which allows the heat to be transported more effectively between the flame front and the unburned mixtures, resulting in faster ignition and propagation.

The comparison between Cantera simulations and experimental data shows that Figure 3 matches the experimental data more closely than Figure 4. This discrepancy in Figure 4 may be attributed to limitations in the GRI-3.0 mechanism for small hydrocarbon chemistry (C1-C4). While the mechanism includes these several reactions for small chemistry, it might have incorrect values or pathways. This could be improved with examinations into the path flux or sensitivity analysis to see which reactions are missing or have incorrect values. By addressing the species and reactions that have the greatest impact on the model, we can increase the accuracy of our model.

Exercise 8: Sensitivity and path flux analysis for methane-air combustion in Cantera

Herman Andersson
23th of July 2025

1. Introduction & Problem

Sensitivity and path flux analysis are critical tools in combustion research for understanding and improving chemical kinetic mechanisms. These analyses provide fundamental insights into the complex network of chemical reactions that govern combustion processes.

Sensitivity analysis is a method used to examine how changes in input parameters of a model affect its outputs. It helps determine which inputs have the most significant influence on the model's results, allowing for future examination and elimination of uncertainties in models. In the case of laminar flame speed, sensitivity analysis determines which individual elementary reaction rates have the biggest effect on the overall speed of propagation.

Path flux analysis (PFA) is a computational method used to simplify complex chemical kinetic mechanisms by identifying and removing less important reaction pathways. It focuses on analyzing the formation and consumption rates of species at different reaction stages to pinpoint crucial pathways.

These methods allow us to focus our attention on improving the model's kinetics around the most influential reactions to ensure a more accurate model. This report will use both of these methods to analyze methane-air combustion in Cantera. The two cases examined will be:

- Perform laminar flame speed sensitivity analysis for methane-air combustion at initial pressures of 1 atm and 20 atm, unburnt gas temperature 298 K, and equivalence ratio 1. All reactions with sensitivity values within -0.03 to 0.03 are plotted and analyzed to identify differences in sensitive reactions between pressure conditions.
- Generate a path flux diagram for methane-air combustion following the conversion of carbon at pressure 1 bar, temperature range 1500-1800 K, and equivalence ratio 1.

2. Theory and Method

2.1 Laminar Flame Speed Sensitivity

Cantera's methods to calculate flame speed sensitivity is through the Normalized flame speed sensitivity s_i . s_i of each reaction in the mechanism is determined with respect to changes in the reaction rate k_i . See equation 1. s_i is calculated with changes in the flame speed S_L when the reaction rate constant k_i changes. The values are normalized through the normalisation factor (denominator in equation) which makes the sensitivities dimensionless and comparable for future analysis.

$$s_i = \frac{\frac{\partial S_L}{\partial k_i}}{\frac{S_L}{k_i}} = \frac{\partial(\ln S_L)}{\partial(\ln k_i)} = \frac{k_i}{S_L} \frac{dS_L}{dk_i} \quad (1)$$

where, s_i - normalized sensitivity value, k_i - rate coefficient, S_L - flame speed

The sensitivity analysis S_i for each reaction is compared to each other to determine the most influential reaction. Positive sensitivity values indicate that increasing the reaction rate enhances flame propagation, while negative values suggest that the reaction inhibits flame speed. Sensitivity values of zero, also called Zero sensitivity, shows that the flame speed is unaffected by the reaction, and thus should not be focused on to improve the model.

Cantera calculates these values through the inbuilt command `get_flame_speed_reaction_sensitivities()`.

2.2 Path Flux Diagram

Cantera uses the open source graph visualization software, Graphviz. Graph visualization is a way of representing structural information as diagrams of abstract graphs and networks. It's used in networking, bioinformatics, software engineering, database and web design, machine learning, and in visual interfaces for other technical domains.

Graphviz layout programs take description of graphs in a simple text language, dot. See figure 1 for structure of DOT language and generated plot from it.

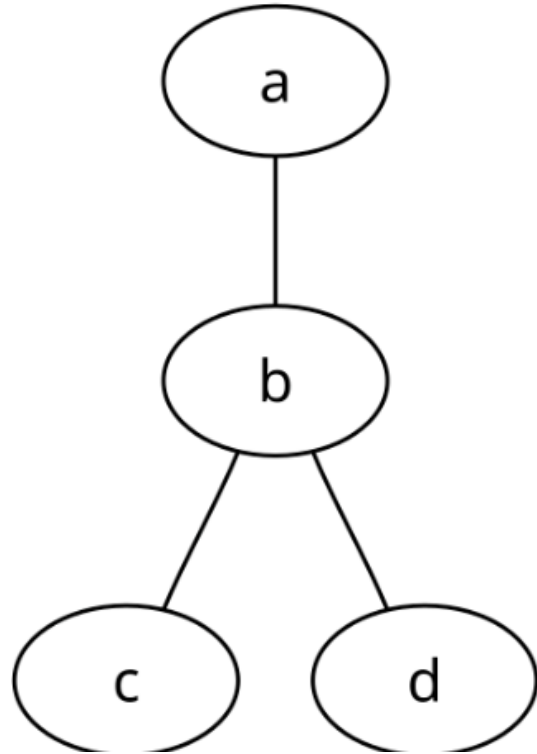


Figure 1: Example of DOT language structure showing undirected and graph representations.

```

// The graph name and the semicolons are optional
graph graphname {
    a -- b -- c;
    b -- d;
}

```

Cantera generates the reaction pathway diagram in dot language, which Graphviz interprets through dot to generate the actual diagram. Cantera's inbuilt function `ct.ReactionPathDiagram(gas, element)`. This creates the reaction path diagram object by analyzing the current gas state and calculating fluxes for the specified element. This is still only saved in the memory. `diagram.write_dot(dot_file)` has to be used to export the analyzed data from memory into a DOT language text file that contains the instructions for Graphviz. `os.system('dot {0} -Tpng -o{1} -Gdpi=300'.format(dot_file, img_file))` is lastly called to generate the the path flux diagram in chosen file type (-Tpng = .png format).

3. Results

From Cantera's calculation and inbuilt commands in the specific two cases, following results were generated.

For the laminar flame speed sensitivity analysis, figure 2 compares the two sensitivity conditions for pressure at 1 atm and 20 atm. The generated laminar flame speed was 37.68 cm/s and 9.86 cm/s for 1 and 20 atm respectively. 1 atm generated 16 sensitive reactions and 20 atm generated 12 that fulfilled the conditions of sensitivity values within -0.03 to 0.03, presented in table 1. Of these reactions, 7 were only found at 1 atm and 2 only at 20 atm, presented in table 2.

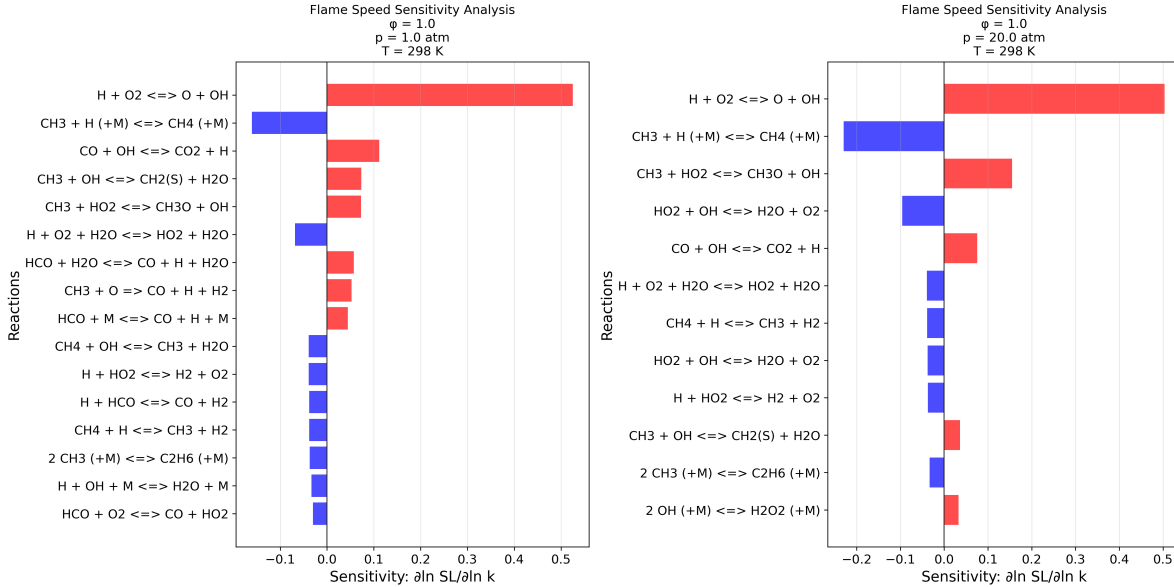


Figure 2: Laminar Flame Speed sensitivity analysis performed for methane-air combustion at initial pressures of 1 atm and 20 atm, unburnt gas temperature 298 K, and equivalence ratio 1. Red shows the reactions with positive sensitivity and blue for negative sensitivity.

Table 1: Sensitivity Analysis Comparison for Methane-Air Combustion

Reaction	1 atm	20 atm
$H + O_2 \rightleftharpoons O + OH$	+0.5254	+0.5035
$CH_3 + H (+M) \rightleftharpoons CH_4 (+M)$	-0.1602	-0.2297
$CO + OH \rightleftharpoons CO_2 + H$	+0.1115	+0.0754
$CH_3 + HO_2 \rightleftharpoons CH_3O + OH$	+0.0724	+0.1549
$CH_3 + OH \rightleftharpoons CH_2(S) + H_2O$	+0.0732	+0.0360
$H + O_2 + H_2O \rightleftharpoons HO_2 + H_2O$	-0.0687	-0.0394
$H + HO_2 \rightleftharpoons H_2 + O_2$	-0.0392	-0.0372
$CH_4 + H \rightleftharpoons CH_3 + H_2$	-0.0380	-0.0392
$2 CH_3 (+M) \rightleftharpoons C_2H_6 (+M)$	-0.0370	-0.0331
$HCO + H_2O \rightleftharpoons CO + H + H_2O$	+0.0575	—
$CH_3 + O \Rightarrow CO + H + H_2$	+0.0523	—
$HCO + M \rightleftharpoons CO + H + M$	+0.0447	—
$CH_4 + OH \rightleftharpoons CH_3 + H_2O$	-0.0393	—
$H + HCO \rightleftharpoons CO + H_2$	-0.0383	—
$H + OH + M \rightleftharpoons H_2O + M$	-0.0334	—
$HCO + O_2 \rightleftharpoons CO + HO_2$	-0.0300	—
$HO_2 + OH \rightleftharpoons H_2O + O_2$	—	-0.0959
$2 OH (+M) \rightleftharpoons H_2O_2 (+M)$	—	+0.0329

Table 2: Pressure-Specific Sensitive Reactions

Only Sensitive at 1 atm	Only Sensitive at 20 atm
$CH_3 + O \Rightarrow CO + H + H_2$	$HO_2 + OH \rightleftharpoons H_2O + O_2$
$HCO + M \rightleftharpoons CO + H + M$	$2 OH (+M) \rightleftharpoons H_2O_2 (+M)$
$H + OH + M \rightleftharpoons H_2O + M$	—
$HCO + H_2O \rightleftharpoons CO + H + H_2O$	—
$CH_4 + OH \rightleftharpoons CH_3 + H_2O$	—
$H + HCO \rightleftharpoons CO + H_2$	—
$HCO + O_2 \rightleftharpoons CO + HO_2$	—

For the Flux path diagram, figure 3 shows the reaction path from our fuel of methane and following the element of carbon. A threshold of 0.02 was chosen to restrict the size of the diagram and still keep the important reactions.

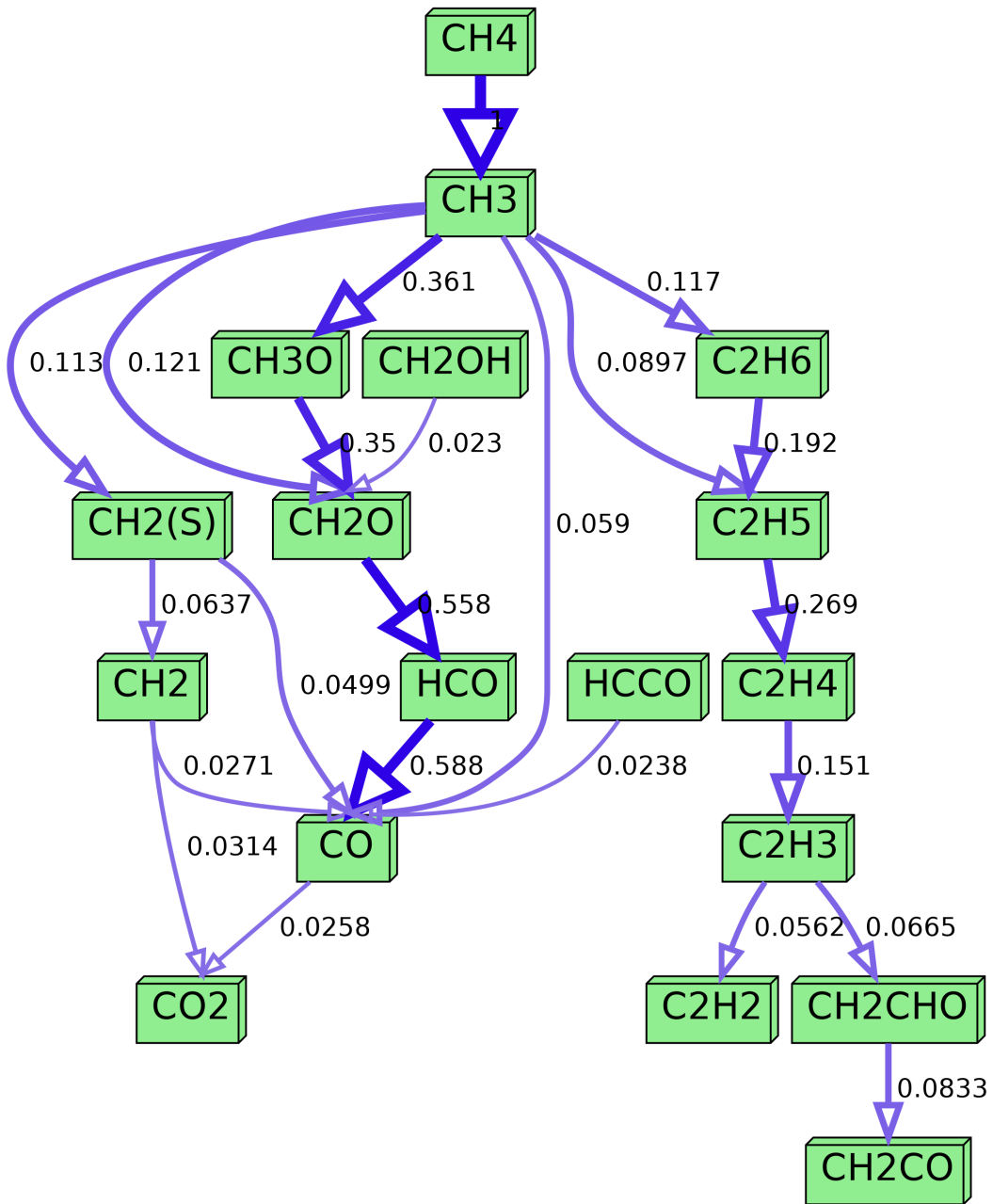


Figure 3: Path flux diagram following Carbon in methane-air combustion carbon at pressure of 1 bar, temperature range 1500-1800 K, and equivalence ratio 1. Green boxes shows the current followed chemical structure and numbers next to arrows show the net flux of the reaction path. All values are normalized against the largest flux.

4. Discussion and Conclusion

From the results we can see several differences between the sensitivity analysis.

Firstly we see that pressure has a large influence on various reaction sensitivities. For example, the reaction $\text{CH}_3 + \text{H} (+\text{M}) \rightleftharpoons \text{CH}_4 (+\text{M})$ (see table 1) shows dramatically different sensitivities. -0.1602 at 1 atm versus -0.2297 at 20 atm. This 43% increase in negative sensitivity demonstrates that pressure dependent reactions become more influential at higher pressures because the increased molecular density enhances three-body collision frequencies.

Three-body reactions require a collision partner (M) for energy and momentum transfer during association reactions, with reaction rates following $\text{Rate} \propto [\text{M}]$. Thus an increase in pressure results in an increased concentration of the collision partner (M), leading to higher reaction rates for termolecular reactions.

An increase in pressure also changes which radical reactions are dominant. The emergence of $\text{HO}_2 + \text{OH} \rightleftharpoons \text{H}_2\text{O} + \text{O}_2$ as a sensitive reaction only at 20 atm (see table 2) illustrates how pressure affects radical reactivity. At higher pressures, HO_2 radicals become more prevalent and reactive as pressure favors the formation of HO_2 in the three body reaction $\text{H} + \text{O}_2 + (\text{H}_2\text{O}) \rightleftharpoons \text{HO}_2 + \text{H}_2\text{O}$ (or the more generalized version $\text{H} + \text{O}_2 + (+\text{M}) \rightleftharpoons \text{HO}_2 + (+\text{M})$). The increased concentration of HO_2 influences the importance of the termination reaction $\text{HO}_2 + \text{OH} \rightleftharpoons \text{H}_2\text{O} + \text{O}_2$ resulting in a negative sensitivity and a reduced laminar flame speed.

We also see the clear effect on the laminar flame speed depending on which types of chain reactions are most influential. Branching reactions, such as $\text{H} + \text{O}_2 \rightleftharpoons \text{O} + \text{OH}$, show clear positive sensitivities and termination reactions, such as $\text{CH}_3 + \text{H} (+\text{M}) \rightleftharpoons \text{CH}_4 (+\text{M})$ shows clear negative sensitivity. For example the dominant branching reaction (and most sensitive of all reactions) at both pressures, $\text{H} + \text{O}_2 \rightleftharpoons \text{O} + \text{OH}$ maintains high positive sensitivity in both cases and therefore is extremely important for model accuracy.

By observing the path flux diagram, we can identify missing important reactions and conclude if we have a relatively good representation of the real reaction pathways. From figure 3, we can identify two important chemicals present which validate the path flux diagram and our choice of tolerance. Firstly, we have a reaction path with several intermediate steps from our fuel CH_4 to CO_2 . CO_2 is the final product of combustion and one of the products present in global reaction theory. We also have a reaction path to C_2H_2 (acetylene), which serves as a critical precursor for soot formation in combustion systems. The presence of C_2H_2 and CO_2 in the path flux diagram not only demonstrates the mechanism's capability to predict realistic combustion intermediates but also enhances the reliability of the pathways by showing consistency with well-established combustion theory and established experimental data.

In conclusion, the appearance of 7 unique reactions at 1 atm and 2 unique reactions at 20 atm indicates that pressure significantly alters the chemical pathways controlling flame propagation. The varying sensitivity values as a function of pressure demonstrate the importance of pressure-specific mechanism validation across different operating conditions. This analysis also serves great importance in the accurate formation of path flux diagrams. The identified reactions from the sensitivity analysis indicate which reactions need to be inspected in the reaction mechanism files (.yaml) and updated with correct kinetic values if they are identified as incorrect. Other methods to ensure the accuracy of the path flux diagram include analysis of correct tolerance settings used in path flux creation. A higher tolerance will result in important reaction pathways being filtered out, while too low tolerance will result in an overabundance of reaction paths that may obscure the dominant chemical routes.

Exercise 9: Development of a mechanism for a methane-air mixture using Reaction Mechanism Generator (RMG)

Herman Andersson
23th of July 2025

1. Introduction & Problem

In combustion modeling, reaction mechanisms are crucial tools for accurately simulating and calculating important characteristics such as laminar flame speed and ignition delay time. In some cases, existing reaction mechanisms can be used, which is the case for methane (CH_4) combustion where GRI-Mech3.0 can be employed. However, in several cases, there is a need to generate custom mechanisms, either because no current reaction mechanism exists or the existing ones do not suit the specific requirements of one's simulation. In these cases, constructing reaction mechanisms by hand is time-consuming, and therefore there is a need for tools such as RMG (Reaction Mechanism Generator) to generate reaction mechanisms efficiently and according to one's specific needs.

In this report, we will use RMG to generate a detailed kinetic mechanism for methane-air combustion and compare the results with GRI-Mech3.0. The conditions for RMG reactor was specified as, pressure of 1 bar, temperature between 700 K to 1400 K and 700 K to 2000 K, equivalence ratio between 0.5 to 1.5 by using initial fractions for ranges of [0.0499, 0.1361] for CH_4 and [0.1815, 0.1996] for O_2 . N_2 was set to 0.71645 and later BalanceSpecies was used to ensure the sum of mole fractions is one. The temperature was The cases we will compare are the following:

- Determine freely propagating laminar flame speed of the RMG-generated mechanism for unburnt mixture temperature 298 K, initial pressure 1 bar and equivalence ratio ranging from 0.5-1.5
- Calculate the ignition delay time for temperatures ranging from 700-1400 K (700-2000K for experimental data comparison) at equivalence ratio 1.1 and pressure 1 bar
- Generate a reaction flux diagram at pressure 1 bar, temperature 1200 K and equivalence ratio 1.1
- Perform flame speed sensitivity analysis for the created mechanism at initial pressure 1 bar, unburnt gas temperature 298 K and equivalence ratio 1.1

The theory behind these calculations and the implementation in Cantera was covered in previous exercises 6, 7, and 8.

2. Theory and Method

2.1 Mechanism Development

The development of chemical kinetic mechanisms is a systematic process that involves multiple stages of refinement and validation. As shown in Figure 1, the process begins with user input defining the desired model conditions, which are then fed into RMG to generate a detailed kinetic model. This initial model undergoes validation against experimental or quantum calculation data to assess its accuracy.

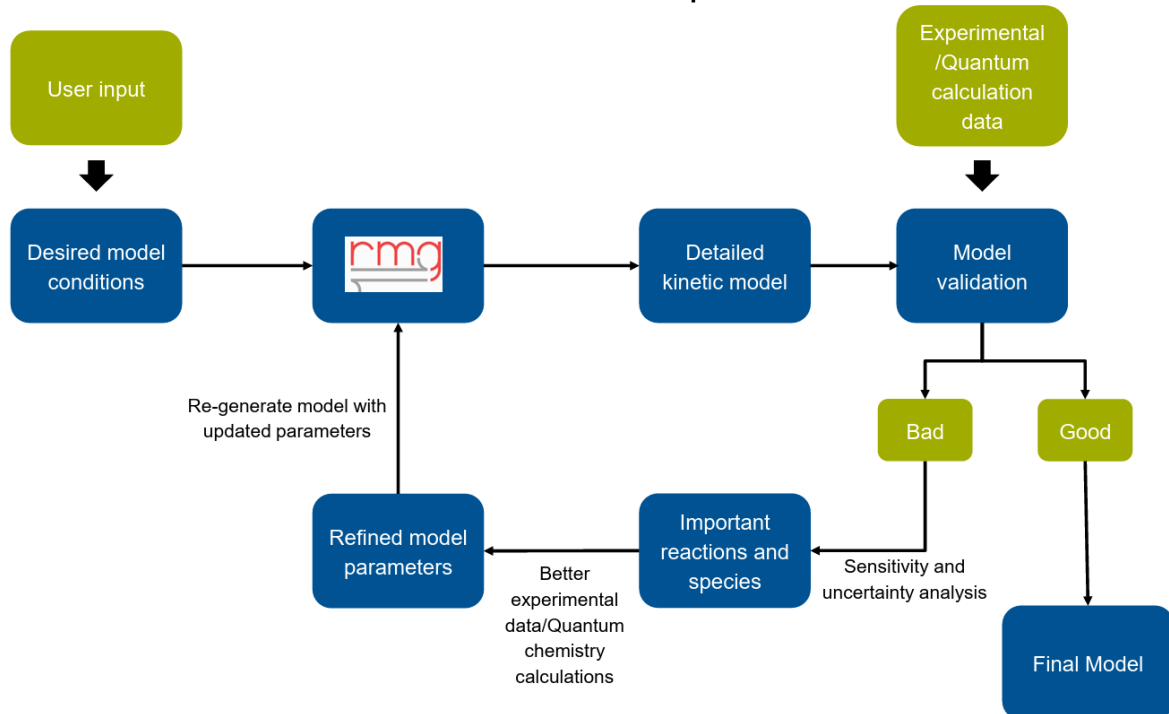


Figure 1: Flow chart illustration of mechanism development.

The validation process determines whether the model is satisfactory or requires further refinement. If the model performs poorly, sensitivity and uncertainty analysis are conducted to identify the most important reactions and species that significantly influence the combustion characteristics. Based on this analysis, better experimental data or quantum chemistry calculations are obtained to refine the model parameters. The updated parameters are then used to regenerate the model. This process is repeated until a satisfactory result is achieved and the model is ready to be used.

2.2 Model generation and expansion in RMG

RMG is an automatic chemical reaction mechanism generator that constructs kinetic models composed of elementary chemical reaction steps using a general understanding of how molecules react. The software employs a systematic approach to mechanism generation through a core-edge methodology.

Initially, reactants are placed at the model core, representing the main mechanism that forms the foundation of the model. All possible reactions are then generated for the species present in the model core. As the generation process continues, new species and reactions are evaluated for inclusion in the core based on conditions defined in the input file, see figure 2

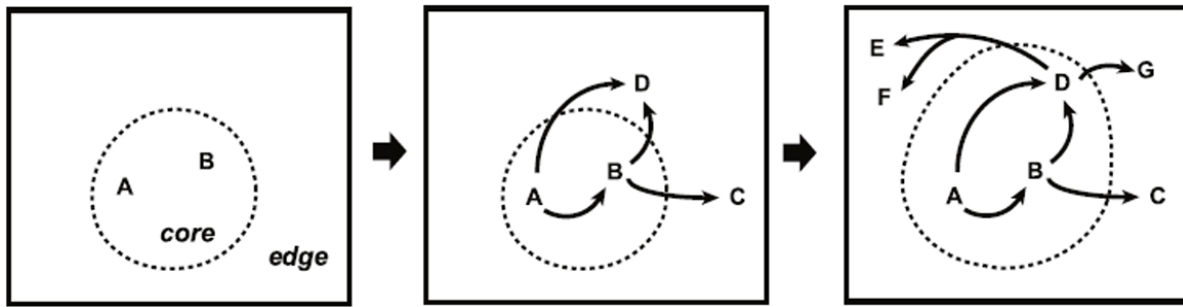


Figure 2: RMG core-edge model generation.

The decision to move species from the edge to the core is based on flux analysis. RMG adds species to the core when the species edge flux $R_i = \frac{dC_i}{dt}$ exceeds εR_{char} , where C_i is the concentration of species i , ε is the tolerance for moving to core, and $R_{char} = \sqrt{\sum_j R_j^2}$ represents the characteristic flux of the system for species j belonging to the core.

Species and reactions that do not meet the specified criteria remain in the model edge, which represents all species and reactions that RMG has produced but are not considered sufficiently important for the current simulation conditions. The core plus edge represents the complete set of species and reactions generated by RMG, while the core alone constitutes the final mechanism used for simulations.

2.3 RMG Input

The RMG input system is structured around several databases and parameters that control mechanism generation. The software follows a hierarchical order of preference for obtaining kinetic and thermodynamic data: seed mechanisms take highest priority, followed by reaction libraries, kinetic depositaries, and finally rate rules. One also needs to add the species information, reactor system, tolerances and dependencies,

The input database consists of several different libraries and reference rules. Kinetics Families define reaction classes such as hydrogen abstraction and unimolecular fuel decomposition. Thermo Libraries provide species thermodynamics data or employ group additivity methods when unavailable. Reaction Libraries contain experimentally validated kinetic parameters. Seed Mechanisms include pre-existing reactions that are automatically incorporated. These are also the base for the model generation as they are added first and highest in the hierarchical order. Kinetics Depositaries store reactions organized by type for rate estimation and Kinetics Estimator specifies methodologies for unknown reaction rates, with the use of models such as rate rules.

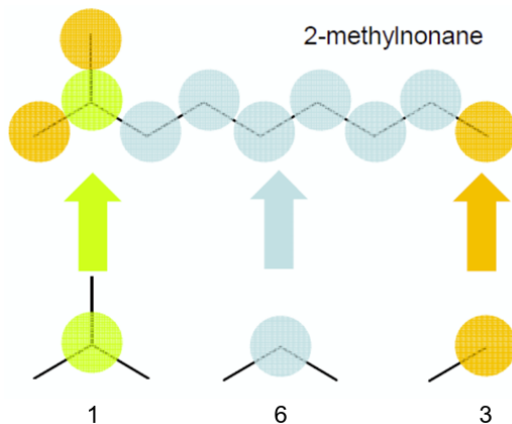


Figure 3: Illustration of Group Additivity theory for larger molecules.

The group additivity method estimates thermodynamic properties by decomposing molecules into functional groups, calculating properties as the sum of group contributions, illustrated in Figure 3. Rate rules use a tree structure to determine unknown kinetic parameters, descending to find the most specific applicable rule or falling back to more general estimates when needed. The drawback with rate rules and why it's often avoided is that rate rules don't take into consideration molecules that have the same molecular formula but with different structures, see figure 4

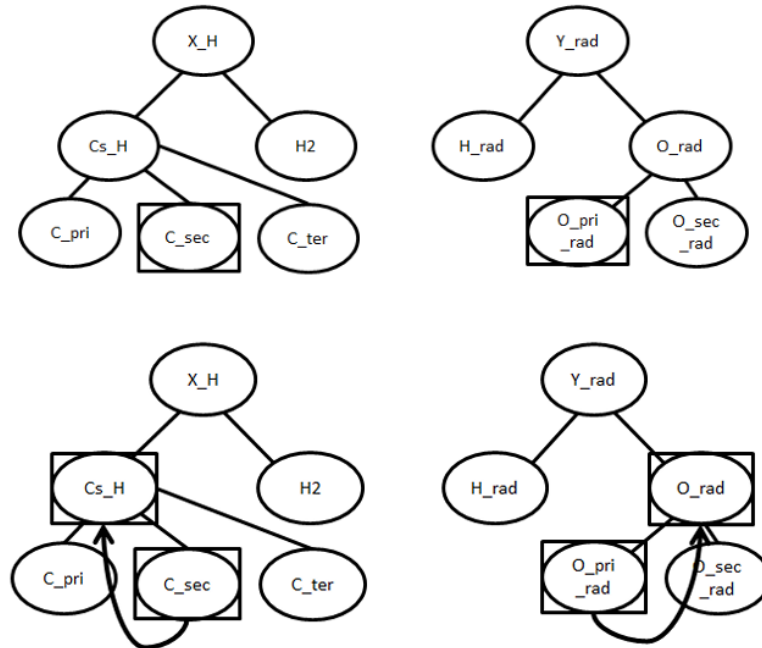


Figure 4: Rate Rules Tree structure for estimating kinetics.

Illustrates the backtracking in rate rules calculating and missing out of key information such as radical placement

Reactant species are defined using SMILES, adjacency lists, or InChI notation, with reactive flags controlling whether species participate in reactions. For example if both O_2 and N_2 are present but O_2 is True and N_2 is False, then we have reactions in air where nitrogen is not participating in the reactions.

The reactor system uses `simpleReactor` for gas-phase isothermal and isobaric conditions. With parameters for temperature/pressure ranges, simulation cycles, and mole fractions. Mole fractions can be added in ranges to calculate over varying equivalence ratios. For this to work one molecule need to be added as single value, otherwise the reactor becomes redundant. For balancing the system. `BalanceSpecies` can be used to ensure the mole fractions adds up to 1. Termination criteria specifies when the generation should stop, can be based either on species conversion (often the fuel is specified) or time limits.

Tolerances control mechanism accuracy: simulator tolerances (`atol`, `rtol`) ensure numerical stability, while model tolerances (`toleranceMoveToCore`, `toleranceInterruptSimulation`, `maximumEdgeSpecies`) determine when species move from edge to core and when simulations are interrupted for model expansion.

Pressure dependence accounts for molecular energy effects at low pressures and high temperatures, with rate coefficients $k(T, P)$ obtained from $k(E)$ using Modified Strong Collision or Reservoir State methods.

Species constraints limit mechanism scope through parameters like `maximumCarbonAtoms`, which limits chemistry up to certain amount of specified atom and `allowed` which allows specified species from lists to bypass previous mentioned constraints.

Output control options include HTML generation for species visualization, statistical plots, CSV simulation profiles,

verbose Chemkin commentary and edge species files. RMG operates exclusively with SI units across all calculations and outputs.

2.4 Model format and duplicate reactions

The final RMG-generated mechanism is typically output in Chemkin format (.cti files), which can be converted to YAML format using Cantera's built-in conversion function. The command `python -m cantera.cti2yaml "<filename>.cti"` performs this conversion. Using the newest version of RMG, this feature is built in, and therefore you immediately generate `chem.yaml` and `chem_annotated.yaml` files.

However, this update does not handle a common problem with duplicate reactions which still needs to be solved to use the mechanism. These duplicates typically arises when the same reaction is represented in multiple ways ((+M) or with specific molecules) or when different rate rules generate similar reactions with slightly different rate parameters. The standard approach to resolve this issue is to retain the more generalized reaction while commenting out or removing the duplicate entries.

3. Results

For the results, three mechanism where generated, one for where the mechanism generation was to be stopped when the fuel (CH_4) reached 95% conversion and the other two when the conversion reached 99%. The difference between the 99% conversion mechanism are that one is generated between 700-1400K and the other one is generated for temperature ranges between 700-2000K. The generated mechanism were compared to the already establishes GRI-Mech3.0 and experimental data. Generation of 95% conversion took around 26 minutes and 99% conversion took around one and a half hour to generate. The re-run of 99% mechanism took 30 minutes with the additional temperature ranges. Amount of species and reactions generated is presented in table 1 for all three mechanisms.

Table 1: Amount of Core species and reactions present in the different mechanisms

Mechanism	Species	Reactions
GRI-Mech 3.0	53	325
RMG 95% conv (700-1400K)	46	779
RMG 99% conv (700-1400K)	45	790
RMG 99% conv (700-2000K)	48	839

Freely propagating laminar flame speed was calculated at 298 K, 1 bar and equivalence ratio ranging from 0.5-1.5 for all three machismen. The experimental data conditions used for comparison where taken during the following conditions, 1 atm, equvilance ratio between 0.65 to 1.25 at unburnt gas temperture of 298 K, see figure 5.

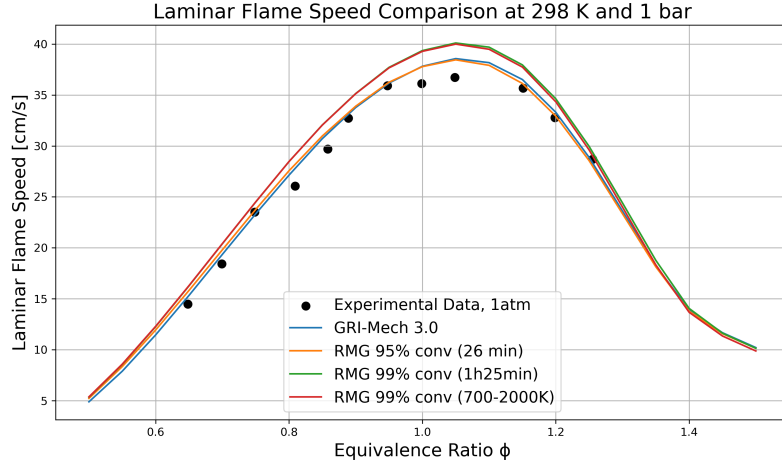


Figure 5: Comparison of Laminar Flame Speed Delay Time between GRI-Mech3.0, 95% conversion, 99% conversion and 99% conversion for 700-2000K. Lines represent Canteras calculations and dots represent the experimental data.

Ignition delay time was calculated at equivalence ratio 1.1; 1 bar and temperatures ranges from 700-2000 K for RMG and between 700-2000 K for GRI-Mech3.0. The experimental data conditions used for comparison were taken during the following conditions, 1 atm, interval between 1500-1950 K and equivalence ratio of 1.0; see figure 6.

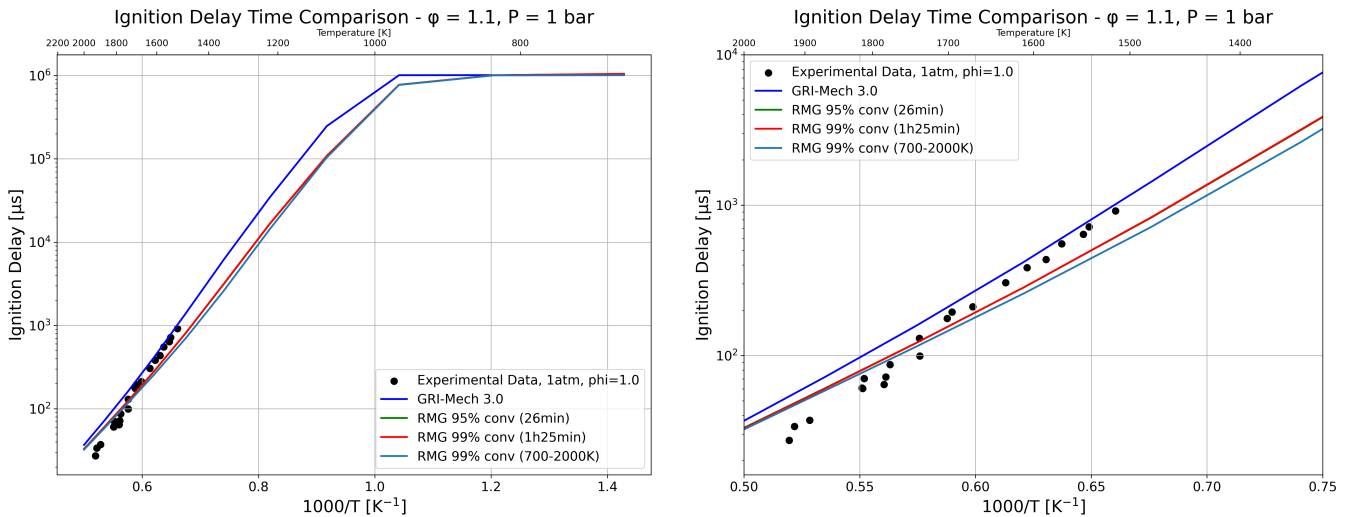


Figure 6: Comparison of Ignition Delay Time between GRI-Mech3.0, 95% conversion, 99% conversion and 99% conversion for 700-2000K. Lines represent Canteras calculations and dots represent the experimental data. Left is the full figure while right plot is zoomed in where the experimental data is present.

For the laminar flame speed sensitivity analysis, figure 7 compares the GRI-Mech3.0 and 99% conversion sensitivity conditions for pressure at 1 bar, unburnt gas temperature 298 K and equivalence ratio 1.1. The generated laminar flame speed was 38.21 cm/s and 39.61 cm/s for GRI-Mech3.0 and 99% conversion (700-2000K) respectively.

GRI-Mech3.0 generated 15 sensitive reactions and RMG generated 14 reactions that fulfilled the conditions of sensitivity values within -0.03 to 0.03, presented in table 2. Of these reactions, only one reaction, $H + HO_2 \rightleftharpoons H_2 + O_2$, was unique to GRI-Mech3.0, RMG had no unique reactions that fulfilled the conditions.

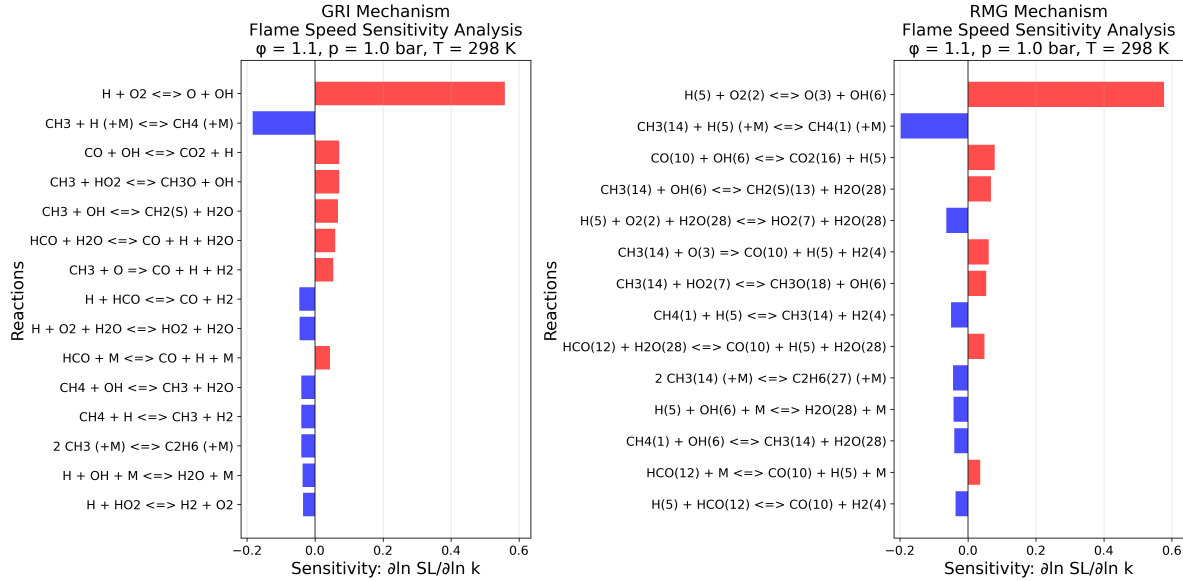


Figure 7: Laminar Flame Speed sensitivity analysis performed for methane-air combustion. Comparison between GRI-Mech3.0 (left) and RMG generated mechanism for 99% conversion (right)

Table 2: Sensitivity Analysis Comparison for Methane-Air Combustion between GRI-Mech3.0 and RMG with 99% conversion (700-2000K)

Reaction	GRI-Mech 3.0	RMG 99%
$H + O_2 \leftrightarrow O + OH$	+0.5586	+0.5767
$CH_3 + H (+M) \leftrightarrow CH_4 (+M)$	-0.1836	-0.1980
$CO + OH \leftrightarrow CO_2 + H$	+0.0715	+0.0786
$CH_3 + HO_2 \leftrightarrow CH_3O + OH$	+0.0711	+0.0542
$CH_3 + OH \leftrightarrow CH_2(S) + H_2O$	+0.0672	+0.0678
$H + O_2 + H_2O \leftrightarrow HO_2 + H_2O$	-0.0451	-0.0637
$HCO + H_2O \leftrightarrow CO + H + H_2O$	+0.0594	+0.0491
$CH_3 + O \Rightarrow CO + H + H_2$	+0.0532	+0.0610
$CH_4 + H \leftrightarrow CH_3 + H_2$	-0.0404	-0.0492
$2 CH_3 (+M) \leftrightarrow C_2H_6 (+M)$	-0.0404	-0.0434
$H + OH + M \leftrightarrow H_2O + M$	-0.0366	-0.0421
$CH_4 + OH \leftrightarrow CH_3 + H_2O$	-0.0405	-0.0400
$HCO + M \leftrightarrow CO + H + M$	+0.0439	+0.0366
$H + HCO \leftrightarrow CO + H_2$	-0.0461	-0.0361
$H + HO_2 \leftrightarrow H_2 + O_2$	-0.0355	—

For the Flux path diagram, figure 8 shows the reaction path from our fuel of methane and following the element of carbon. A threshold of 0.02 was chosen to restrict the size of the diagram and still keep the important reactions.

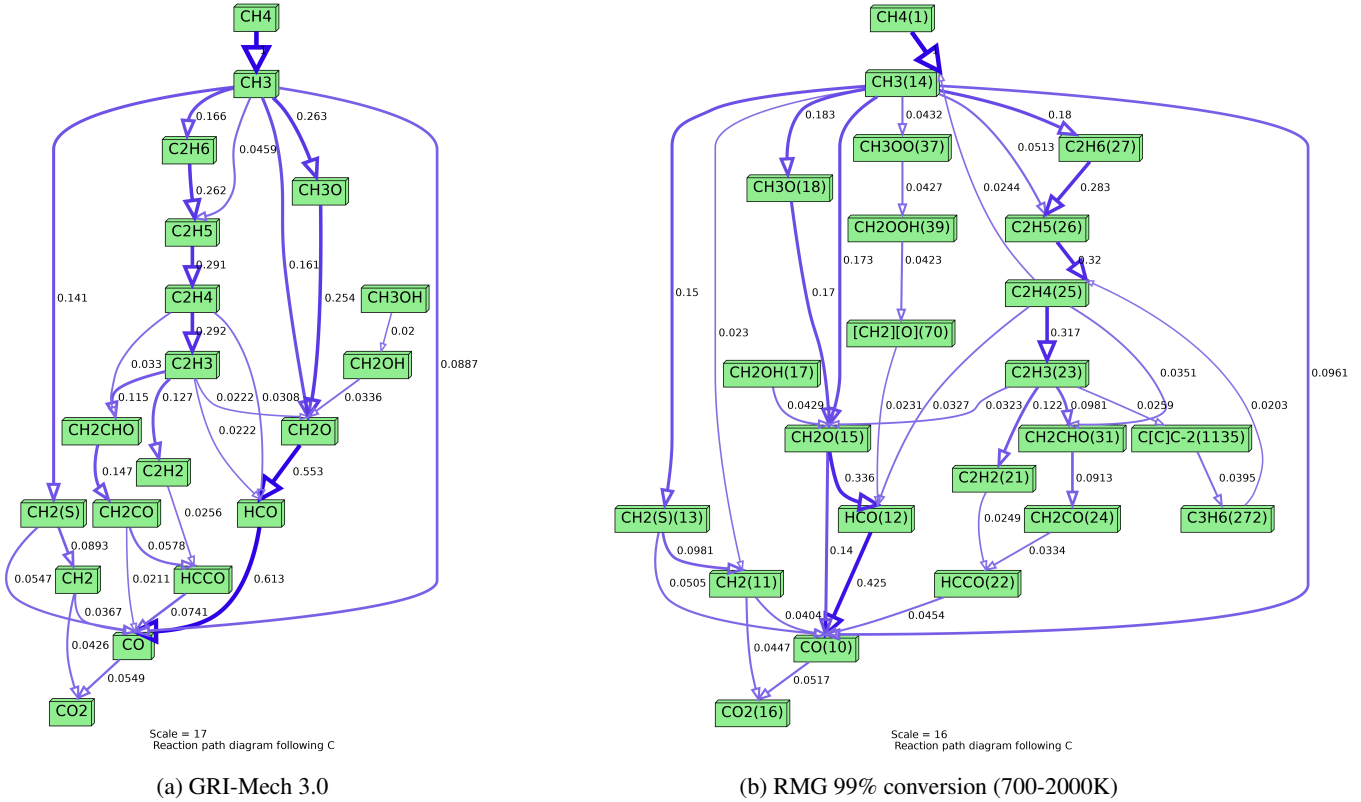


Figure 8: Path flux diagrams following Carbon in methane-air combustion at pressure of 1 bar, temperature range 1200-1800 K, and equivalence ratio 1.1: Green boxes show the current followed chemical structure and numbers next to arrows show the net flux of the reaction path. All values are normalized against the largest flux.

4. Discussion and Conclusion

Despite the RMG-95% conversion mechanism showing better overall agreement with GRI-Mech3.0 in laminar flame speed calculations, the RMG-99% conversion mechanism was selected for sensitivity analysis and reaction path flux diagrams. This decision was based on the principle that a more complete mechanism (99% conversion) would provide a more comprehensive representation of chemical kinetics for reaction pathways, minimizing the chances of missing minor but important reactions that might provide insight into rate-controlling steps during sensitivity analysis. Maximizing combustion through a more complete combustion is also the preferred answer in industrial and academic applications. The updated temperature range mechanism for the conversion of 99% was used to ensure that the mechanism was designed to calculate the ranges of our experimental data in the intervals.

4.1 Laminar Flame Speed

The laminar flame speed comparison in figure 5, shows that GRI-Mech3.0 and RMG-95% generate similar values, with greater differences observed at higher and lower equivalence ratios, which also matches the experimental data well. RMG-99% shows a similar structure to the other mechanisms but overshoots the flame speed values. The difference between RMG-95% and RMG-99% (1400K) is one species and 11 reactions with RMG-99% (2000K) adding additional 50 reactions. As both RMG-99% shows almost identical LFS-values and overshoot, there is reasonable conclusion that the 11 additional reactions between 95% and 99% for the lower temperature mechanism is the likely reason for this overshoot. Investigating whether these reactions originate from one of the libraries or were generated by group additivity or rate rules could result in

improved kinetic values and a more accurate model, especially since rate rules might ignore important molecular structures.

4.2 Ignition Delay Time

The ignition delay time in figure 6 shows a clear difference between GRI-Mech3.0 and the RMG-generated mechanisms, with all RMG conversions showing shorter ignition delay times (IDT) for the same temperature. A likely reason for RMG's faster response can be seen table 1, where RMG is missing the termination reaction $H + HO_2 \rightleftharpoons H_2 + O_2$, which lowers the IDT value as radical termination reactions decrease the amount of radicals present in the system.

It can also be observed that all mechanisms reach a plateau at IDT = 1s. This is a numerical limitation in the code where the estimated ignition time acts as a hard limit for the generated IDT. The estimated IDT value would need to be increased to 1000 s to avoid this plateau. Results at low temperatures are not reliable as GRI-Mech3.0 was designed for temperatures above 1000 K. RMG, which uses GRI-Mech3.0 as a base in thermoLibraries, reactionLibraries, and as a seed mechanism, inherits these limitations and must rely on group additivity and rate rules at such low temperatures. For improved low-temperature performance, specialized mechanisms or kinetic data designed for these conditions would be required.

4.3 Sensitivity Analysis

The sensitivity analysis comparison between GRI-Mech3.0 and RMG-99% (2000K) shows great similarity in identifying rate controlling reactions. Both mechanisms identify the same critical reactions, with $H + O_2 \rightleftharpoons O + OH$ showing the highest positive sensitivity coefficient (0.5586 for GRI and 0.5767 for RMG-99%), confirming this reaction's role as the primary chain-branching step.

The $CH_3 + H (+M) \rightleftharpoons CH_4 (+M)$ reaction shows the strongest negative sensitivity in both mechanisms (-0.1836 for GRI and -0.1980 for RMG-99%), indicating its role in chain termination.

While the top three most sensitive reactions remain the same in both mechanisms, some changes in importance order can be noticed among the other sensitive reactions, though they still present similar sensitivity values to GRI.

As mentioned above, the biggest difference is the absence of the $H + HO_2 \rightleftharpoons H_2 + O_2$ reaction from the RMG-99% mechanism's sensitivity list.

4.4 Reaction Path Analysis

The overall reaction path flux is similar for both GRI-Mech3.0 and RMG-99% (2000K), with RMG-99% containing more reaction pathways as a result of having more than twice the number of reactions compared to GRI-Mech3.0. Both mechanisms contain similar reaction paths from the fuel (CH_4) to the end products of CO_2 and important species such as C_2H_2 (acetylene) to confirm the reliability.

The variation in scale and normalized fluxes can also be contributed to the additional reaction pathways. One clear example of the differences is the additional reaction branch containing $CH_3OO(37)$, $CH_2OOH(39)$, and $[CH_2]O(70)$, which is not present in GRI-Mech3.0.

4.5 Conclusions

The differences between GRI-Mech3.0 and RMG's mechanisms can be attributed to the increased number of reactions present in RMG compared to GRI-Mech3.0. Since GRI-Mech3.0 serves as the seed and first library in many of RMG's databases, the fundamental reactions originate from GRI-Mech3.0, while newly generated reactions (over 300) likely obtain their kinetics from group additivity and rate rules, which might provide incorrect values as observed in the laminar flame

speed results. This explains why the path flux and sensitivity analyses are similar for both RMG and GRI-Mech3.0, as the fundamental chemistry is comparable.

For better model accuracy, RMG would need to examine both the reactions added between RMG-95% and RMG-99% to understand how they affected the laminar flame speed predictions. The mechanism would also require investigating the reactions that the sensitivity analysis identified, especially $H + HO_2 \rightleftharpoons H_2 + O_2$, to determine if these kinetic values are accurate or need adjustment according to the literature. These corrections are post-fixes and would work to ensure our model fits our experimental data, but might lack aspects for scientific uses as the model could potentially leave out important kinetics for understanding the reactions. Thus, another approach of looking into the chemistry of the whole reaction and updating the input file in accordance with important chemical reaction pathways and radicals which might have been left out previously to ensure that RMG generates an accurate model. This would allow us to generate mechanisms for other reactor conditions and avoid the post-work of checking kinetic values and thus reduce the amount of work needed to be done manually.

Exercise 10: Reduction of a kinetic mechanism using pyMARS

Herman Andersson
23th of July 2025

1. Introduction & Problem

In combustion modeling, detailed kinetic mechanisms are essential for understanding fundamental combustion characteristics, but their computational complexity often limits their practical application in large-scale simulations. Detailed mechanisms can contain hundreds of species and thousands of reactions that accurately predicts behavior in combustion. However, as all of these reactions and species are not relevant for the overall behavior, effective reduction methods can be used to reduce the mechanisms while still retaining accurate modeling data. Thus, drastically lowering the computational cost of these models.

In this report, we employ pyMARS (Python-based Mechanism Automatic Reduction Software) to reduce the GRI-Mech3.0 kinetic mechanism for methane-air combustion. We will use Directed Relation Graph with error propagation (DRGEP) with initial sensitivity analysis (DRGEPSA). The reduction will be performed under specified conditions of 1 atm pressure, reactor temperature ranging from 700-2000 K and equivalence ratio of 1.1: The reduced model will be compared with the unchanged GRI-Mech3.0 and the generated RMG mechanism from exercise 9. The cases for comparison are

- Ignition Delay Time for 1 bar, temperature ranging from 700-2000 K and equivalence ratio of 1.1:
- Laminar Flame Speed for 1 bar, temperature of unburnt gas mixture at 298 K and equivalence ratio between 0.5 to 1.5:

2. Theory and Method

2.1 Mechanism Reduction Fundamentals

Mechanism reduction techniques are categorized by their approach to identifying and eliminating less important species and reactions. The primary methods include sensitivity analysis, detailed reduction, computational singular perturbation (CSP), and directed relation graph (DRG) approaches. Each method balances performance against computational cost, with more sophisticated techniques generally providing better reduction quality at higher computational expense. Figure 1 shows an overview of the performance against computational cost for different reduction techniques.

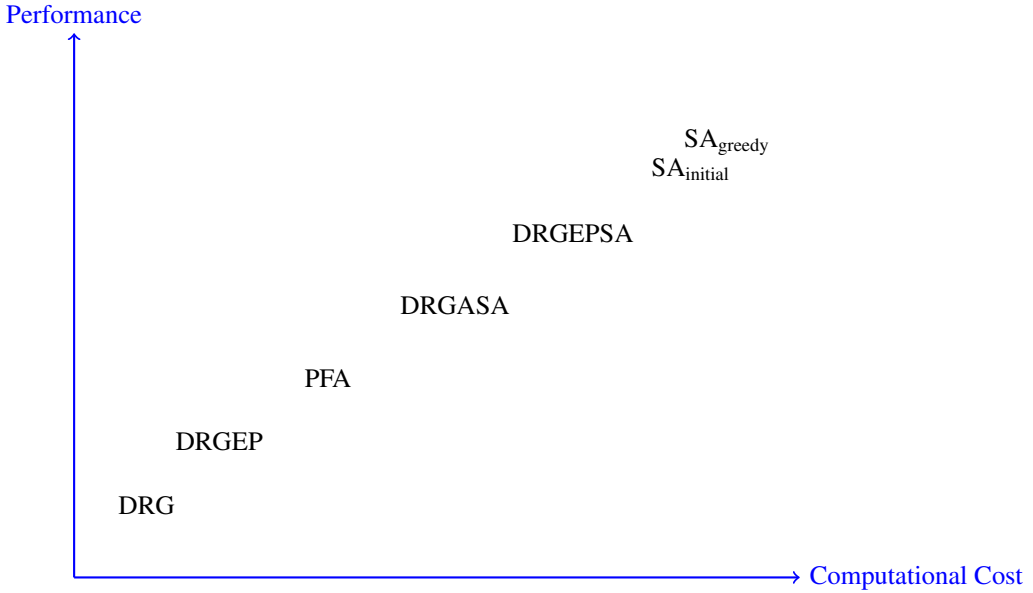


Figure 1: Performance vs computational cost comparison of different mechanism reduction methods

The reduction techniques can remove important and wanted reactions as well as make the mechanism unreliable with a too high error rate. Retained species, threshold and error limit values needs to be specified according to know theory in order to ensure the accuracy of the reduced model.

2.2 Directed Relation Graph (DRG)

The DRG method identifies and eliminates species of negligible importance by calculating interaction coefficients between target species and candidate species for removal. For a target species A, the method calculates the interaction coefficient (r_{AB}) representing the production rate dependency of A on species B, see equation (1)

$$r_{AB} \equiv \frac{\sum_{k=1,K} |\nu_{A,k} \omega_k \delta(B)_k|}{\sum_{k=1,K} |\nu_{A,k} \omega_k|} \quad (1)$$

$$\text{where } \delta(B)_k = \begin{cases} 1, & \text{if the } k^{\text{th}} \text{ elementary reaction involves species B} \\ 0, & \text{otherwise} \end{cases}$$

The parameters $\nu_{A,k}$ represents the stoichiometric coefficient of species A in the k^{th} elementary reaction, ω_k is the overall rate of reaction for K, and K is the total number of reactions. If $r_{AB} < \varepsilon$ (cutoff threshold), species B is removed from the mechanism, provided this removal does not eliminate reactions essential for important pathways. Meaning that an unimportant reaction will not be removed in case it's necessary to produce another species which has an important reaction. For example in figure 2, if reaction $A \Rightarrow B$ is unimportant, but $B \Rightarrow C$ is. Then $A \Rightarrow B$ will remain as it solely produce species B which is necessarily for the important reaction of $B \Rightarrow C$.

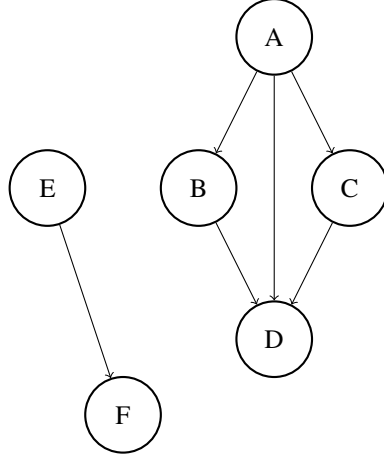


Figure 2: Reaction pathways, connections between different species in Directed Relation Graph theory

2.3 Directed Relation Graph with Error Propagation (DRGEP)

DRGEP represents an improved version of DRG that better accounts for indirect species dependencies through graph pathways. In figure 2, we see that A is directly affects B,C and D, but also effects D indirectly through $A \Rightarrow B \Rightarrow D$ and $A \Rightarrow C \Rightarrow D$

DRGEP uses the overall interaction coefficients (R_{AB}) to decide which species to keep. (R_{AB}) is calculated with the maximum product for all paths between the chosen two species, see equation (2)

$$R_{AB} = \max_{\text{all paths } p} (r_{AB,p}) \quad (2)$$

Where the updated formula for interaction coefficients (r_{AB}) is calculated thorough equation (3)

$$r_{AB} = \frac{\sum_{k=1,K} |\nu_{A,k} \omega_k \delta(B)_k|}{\max(P_A, C_A)} \quad (3)$$

$P_A = \sum_{k=1,K} \max(0, \nu_{A,k} \omega_k)$ represents production and $C_A = \sum_{k=1,K} \max(0, -\nu_{A,k} \omega_k)$ represents consumption. $r_{AB,p} = \prod_{j=1}^{n-1} r_{s_j s_{j+1}}$ is used to calculates the paths for n species between A and B.

So for figure 2, R_{AB} would be calculated according to equation (4)

$$R_{AB} = \max_{\text{all paths } p} (r_{ad,p}) = \max(r_{AD,1}, r_{AD,2}, r_{AD,3}) = \max(r_{AB} r_{BD}, r_{AD}, r_{AC} r_{CD}) \quad (4)$$

2.4 Sensitivity Analysis Integration

Due to the high computational cost of sensitivity analysis, it is typically applied in combination with DRG or DRGEP methods. The combined approaches (DRGASA and DRGEPSA) first remove a significant fraction of species using graph-based methods, then apply sensitivity analysis to the smaller mechanism.

Two sensitivity analysis algorithms are implemented in pyMARS:

Initial Algorithm: Error induced by limbo species removal is evaluated once at the beginning, with species considered for removal in ascending order of induced error.

Greedy Algorithm: The induced error of remaining limbo species is re-evaluated after each removal, selecting the species with the lowest induced error at each step.

2.5 pyMARS Implementation

pyMARS requires input files in cti format specifying the detailed mechanism, target species, retained species, reduction method, error limits, and reactor conditions. The software implements various reduction methods with different performance-cost trade-offs, from simple DRG to computationally expensive sensitivity analysis approaches.

Key input parameters include:

- Detailed mechanism (RMG-generated mechanism or GRI-Mech3.0)
- Target species (fuel, oxidizer)
- Retained species (species that must remain in reduced mechanism, such as CO₂ and intermediate species)
- Reduction method specification (DRG, DRGEP, with or without sensitivity analysis)
- Error tolerance limits for the reduced model (Maximum acceptable deviation between detailed and reduced mechanism predictions.)
- Threshold values for species interaction coefficients (ε -value, removed from model if R_{AB} or r_{AB} is lower)
- Reactor conditions (temperature, pressure, equivalence ratio ranges)

pyMARS evaluates mechanism accuracy based on ignition delay time rather than laminar flame speed. The software systematically removes species while monitoring error accumulation to ensure the reduced mechanism remains within specified accuracy bounds.

3. Results

For the results, two reduced .cti files were generated from pyMars reduction of GRI-Mech3.0, R-17 and R-24. The two reduced mechanism were compared to the already established GRI-Mech3.0, our previously generated RMG-mechanism from exercise 9 and experimental data. Amount of species and reactions generated is presented in table 1 for all four mechanisms.

Table 1: Amount of Core species and reactions present in the different mechanisms

Mechanism	Species	Reactions
GRI-Mech 3.0	53	325
RMG 99% conv (700-2000K)	48	839
GRI reduced 17 (R-17)	17	58
GRI reduced 24 (R-24)	24	102

Freely propagating laminar flame speed was calculated at 298 K, 1 bar and equivalence ratio ranging from 0.5-1.5 for all four mechanism. The experimental data conditions used for comparison were taken during the following conditions, 1 atm, equivalence ratio between 0.65 to 1.25 at unburnt gas temperature of 298 K, see figure 3.

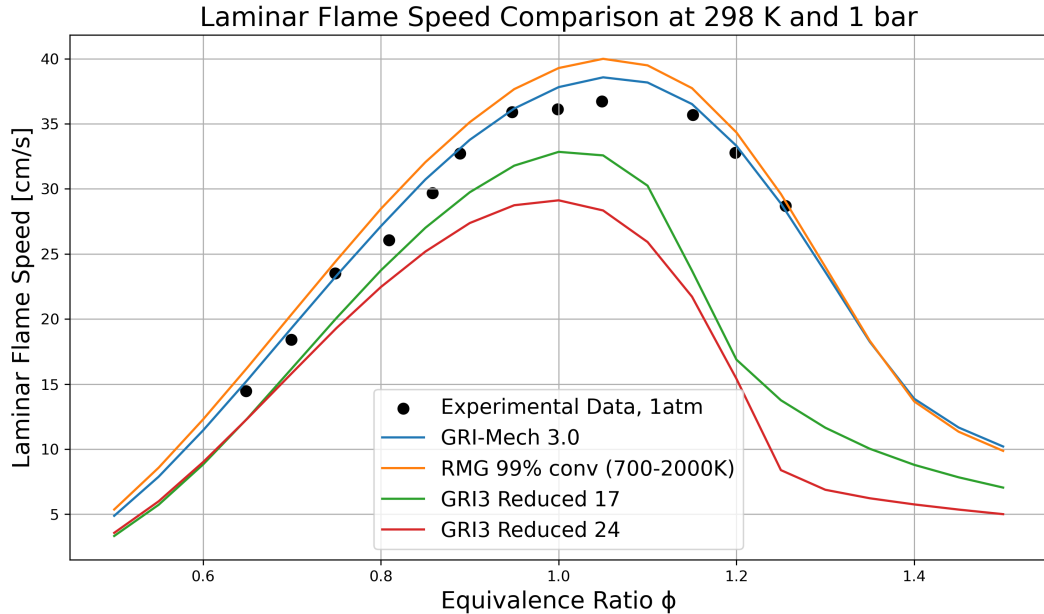


Figure 3: Comparison of Laminar Flame Speed Delay Time between GRI-Mech3.0, RMG-mechanism, R-17 and R-24. Lines represent Cantera calculations and dots represent the experimental data.

Ignition delay time was calculated at equivalence ratio 1.1; 1 bar and temperatures ranges from 700-2000 K. The experimental data conditions used for comparison were taken during the following conditions, 1 atm, interval between 1500-1950 K and equivalence ratio of 1.0; see figure 4.

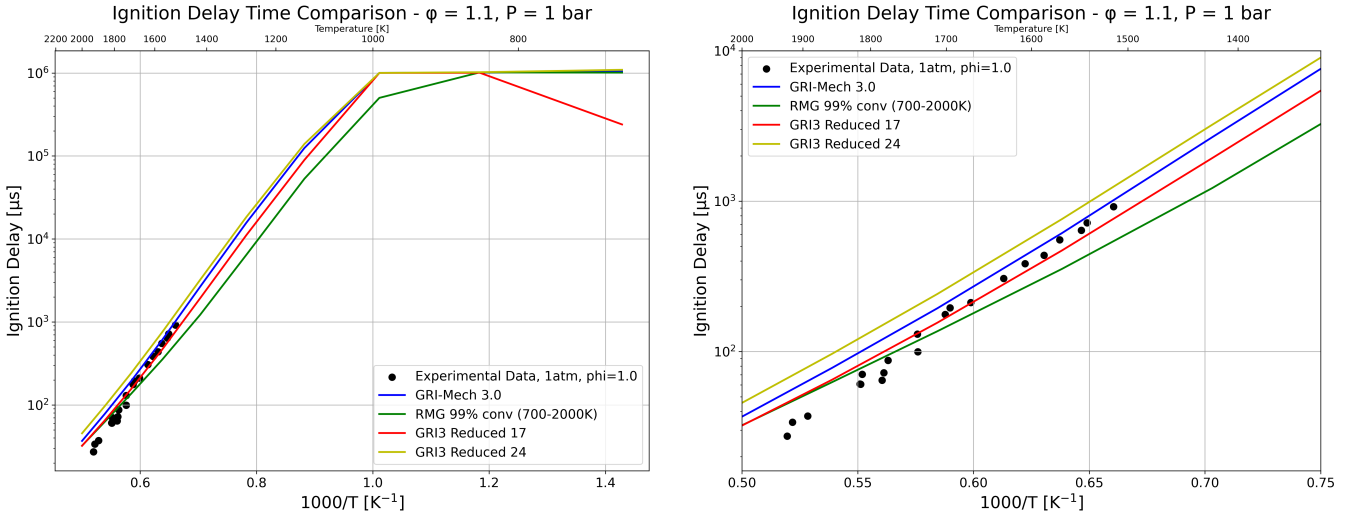


Figure 4: Comparison of Laminar Flame Speed Delay Time between GRI-Mech3.0, RMG-mechanism, R-17 and R-24. Lines represent Canteras calculations and dots represent the experimental data. Left is the full figure while right plot is zoomed in where the experimental data is present.

A laminar flame speed sensitivity analysis was performed to compare R-17 and R-24 and GRI-Mech3.0, presented in figure 5 was performed for pressure at 1 bar, unburnt gas temperature 298 K and equivalence ratio 1.1. The generated laminar flame speed was 38.21 cm/s for GRI-Mech3.0, 30.30 cm/s for R-17, 25.92 cm/s for R-24 and 39.80 cm/s for RMG 99% conversion.

R-17 generated 14 and R-24 generated 21 sensitive reactions respectively. These reactions are compared to the top 15 sensitivity reactions in the GRI-Mech3.0 mechanism that fulfilled the conditions of of sensitivity values within -0.03 to 0.03, presented in table 2. In table ?? the sensitivity reactions between R-17 and R-24 are compared.

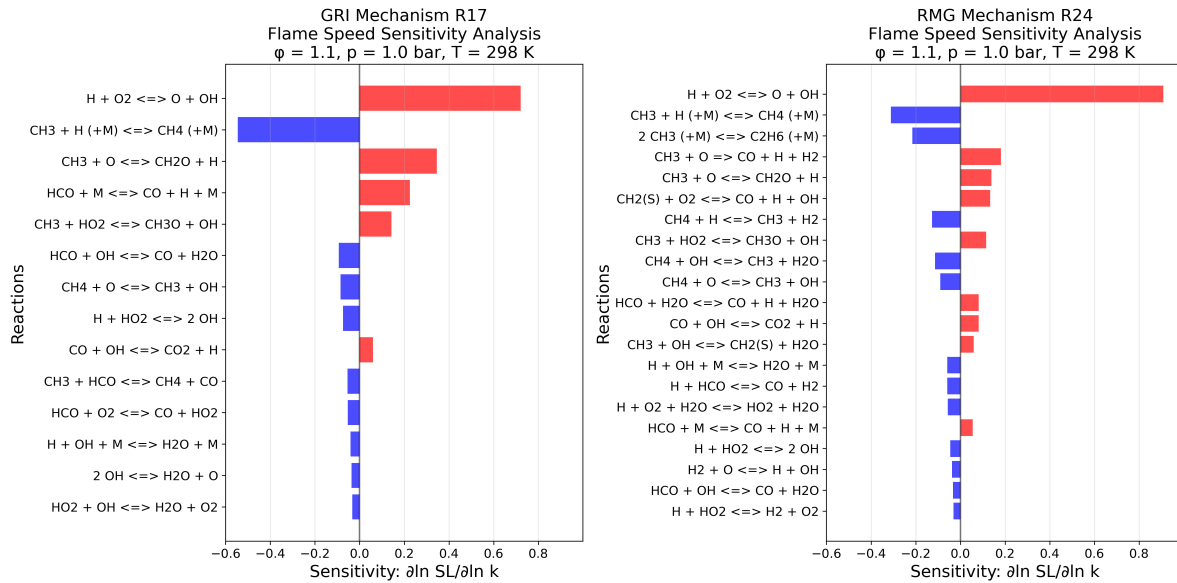


Figure 5: Laminar Flame Speed sensitivity analysis performed for methane-air combustion. Comparison between GRI-Mech3.0 (left) and RMG generated mechanism for 99% conversion (right)

Table 2: Sensitivity Analysis Comparison for Methane-Air Combustion between GRI-Mech3.0, RMG with 99% conversion, R-17 and R-24

Reaction	GRI-Mech 3.0	RMG 99%	GRI-R17	GRI-R24
$H + O_2 \rightleftharpoons O + OH$	+0.5586	+0.5715	+0.7210	+0.9085
$CH_3 + H (+M) \rightleftharpoons CH_4 (+M)$	-0.1836	-0.1983	-0.5459	-0.3112
$CO + OH \rightleftharpoons CO_2 + H$	+0.0715	+0.0786	+0.0596	+0.0814
$CH_3 + HO_2 \rightleftharpoons CH_3O + OH$	+0.0711	+0.0533	+0.1424	+0.1151
$CH_3 + OH \rightleftharpoons CH_2(S) + H_2O$	+0.0672	+0.0669	—	+0.0594
$H + O_2 + H_2O \rightleftharpoons HO_2 + H_2O$	-0.0451	-0.0633	—	-0.0569
$HCO + H_2O \rightleftharpoons CO + H + H_2O$	+0.0594	+0.0488	—	+0.0816
$CH_3 + O \Rightarrow CO + H + H_2$	+0.0532	+0.0598	—	+0.1817
$CH_4 + H \rightleftharpoons CH_3 + H_2$	-0.0404	-0.0470	—	-0.1268
$2 CH_3 (+M) \rightleftharpoons C_2H_6 (+M)$	-0.0404	-0.0416	—	-0.2150
$H + OH + M \rightleftharpoons H_2O + M$	-0.0366	-0.0418	-0.0405	-0.0593
$CH_4 + OH \rightleftharpoons CH_3 + H_2O$	-0.0405	-0.0383	—	-0.1136
$HCO + M \rightleftharpoons CO + H + M$	+0.0439	+0.0364	+0.2254	+0.0546
$H + HCO \rightleftharpoons CO + H_2$	-0.0461	-0.0357	—	-0.0584
$H + HO_2 \rightleftharpoons H_2 + O_2$	-0.0355	—	—	-0.0311

Table 3: Sensitivity Analysis Comparison for Methane-Air Combustion between reduced mechanism R-17 and R-24

Reaction	GRI-R17	GRI-R24
$H + O_2 \rightleftharpoons O + OH$	+0.7210	+0.9085
$CH_3 + H (+M) \rightleftharpoons CH_4 (+M)$	-0.5459	-0.3112
$CH_3 + O \rightleftharpoons CH_2O + H$	+0.3460	+0.1385
$HCO + M \rightleftharpoons CO + H + M$	+0.2254	+0.0546
$2 CH_3 (+M) \rightleftharpoons C_2H_6 (+M)$	—	-0.2150
$CH_3 + O \Rightarrow CO + H + H_2$	—	+0.1817
$CH_3 + HO_2 \rightleftharpoons CH_3O + OH$	+0.1424	+0.1151
$CH_2(S) + O_2 \rightleftharpoons CO + H + OH$	—	+0.1337
$CH_4 + H \rightleftharpoons CH_3 + H_2$	—	-0.1268
$CH_4 + OH \rightleftharpoons CH_3 + H_2O$	—	-0.1136
$HCO + OH \rightleftharpoons CO + H_2O$	-0.0936	-0.0329
$CH_4 + O \rightleftharpoons CH_3 + OH$	-0.0849	-0.0898
$HCO + H_2O \rightleftharpoons CO + H + H_2O$	—	+0.0816
$CO + OH \rightleftharpoons CO_2 + H$	+0.0596	+0.0814
$CH_3 + OH \rightleftharpoons CH_2(S) + H_2O$	—	+0.0594
$H + OH + M \rightleftharpoons H_2O + M$	-0.0405	-0.0593
$H + HCO \rightleftharpoons CO + H_2$	—	-0.0584
$H + O_2 + H_2O \rightleftharpoons HO_2 + H_2O$	—	-0.0569
$CH_3 + HCO \rightleftharpoons CH_4 + CO$	-0.0543	—
$HCO + O_2 \rightleftharpoons CO + HO_2$	-0.0527	—
$H + HO_2 \rightleftharpoons 2 OH$	-0.0747	-0.0454
$H_2 + O \rightleftharpoons H + OH$	—	-0.0376
$2 OH \rightleftharpoons H_2O + O$	-0.0359	—
$HO_2 + OH \rightleftharpoons H_2O + O_2$	-0.0329	—
$H + HO_2 \rightleftharpoons H_2 + O_2$	—	-0.0311

4. Discussion and Conclusion

In figure 3, we clearly see that the reduced mechanism follows the same trend but lower LFS-value than the original GRI-Mech3.0 mechanism until $\varphi = 1.1$ where the laminar flame speed value starts to drop. This trend does not follow the experimental data, so the reduced mechanism has lost severe accuracy.

In contrast to the IDT-calculations, seen in figure 4. Where the reduced mechanism follows the same trend as GRI-Mech3.0 with the variation that R-17 undershoots and R-24 overshoots in comparision to GRI-Mech3.0.

The over- and undershoot of IDT calculations is most likley due to what type of reactions where left in the reduced mechanism. As seen in table 2 and table 3 that R-24 includes more chain termination reactions such as $2 \text{CH}_3 (+\text{M}) \leftrightarrow \text{C}_2\text{H}_6 (+\text{M})$. This increase in chain termination and lack of branching and propagation in comparison would explain why R-24 overshoots the IDT and R-17, which lacks these terminations reactions, would undershoot and have a lower IDT value than the base mechanism.

The reason why IDT still provides accurate values and LFS loses a great deal of accuracy even though they contain the same sensitivity reactions according to table 2, is most likely because the least important reactions that were removed in the reduction still serve a purpose and have an impact on the LFS value.

This happens because pyMars is currently designed to calculate its error rate according to IDT. pyMars uses Autoignition parameters to sample its thermochemical data and bases which species and reactions should remain. As a result, pyMars considers IDT and not LFS for the reducing, which will result in IDT still being fairly accurate while LFS can have severe accuracy damages which pyMars simply ignores. There is currently implements ongoing to update pyMars to include LFS in it's error calculations. These implements are currently not available and thus we get this error.

This is the cost of using reduction tools such as pyMars. The computational cost is dropped and the mechanism becomes more available for practical applications. However, it loses its accuracy, and in some cases like this, completely makes the mechanism unusable in some areas. This can be minimized with theory and improved reduction tools, but the problem will always remain there. There will always be a trade off between accuracy and practicality.